Binuclear Xanthate Macrocyclic Complexes of Co^{II}, Ni^{II}, Cu^{II} and Zn^{II} Derived from *N*-Substituted Diethanol Amine, CS_2 and $M(OAc)_2$: Synthesis, Characterization, DFT study and *in vitro* Cytotoxic Activity

Abstract

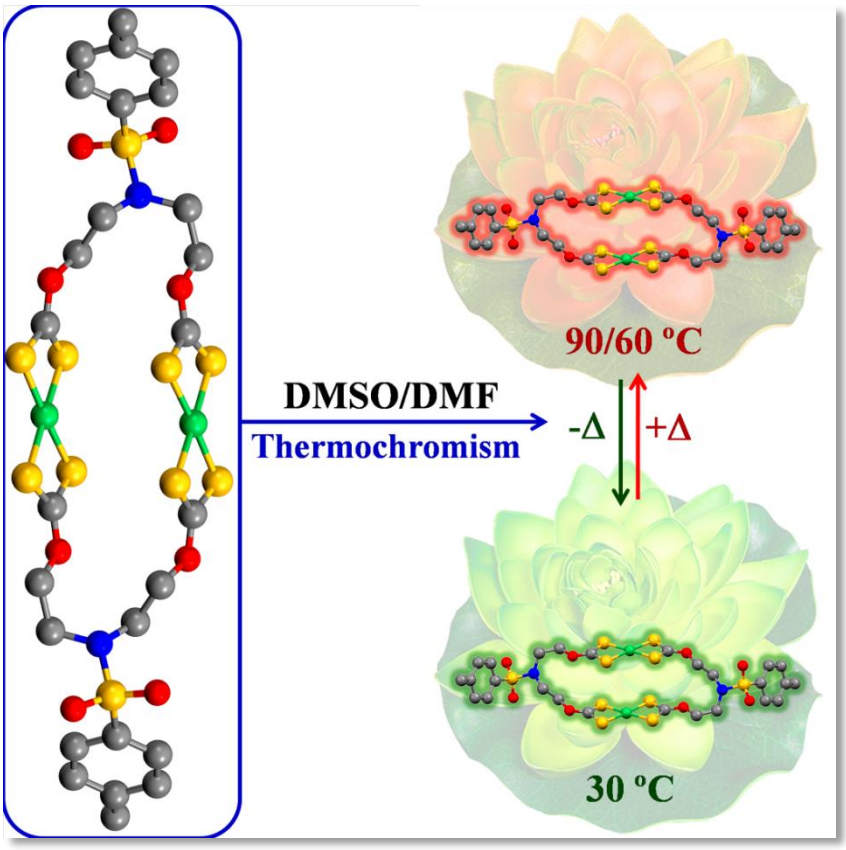

Novel series of binuclear metallamacrocyclic complexes of type [M^{II}_2-μ^2-bis-{(κ^2S,S-$S_2COCH_2CH_2)_2N(R)$}] **1-8** have been efficiently synthesized in a one-pot self-assembly process. Interestingly, complex **4** is utilized to synthesize a macrocyclic compound, 6,14-ditosyl-1,3,9,11-tetraoxa-6,14-diaza-cyclohexadecane-2,10-dithione (**9**), which is extremely difficult to synthesize conventionally. Compounds 2 and 9 have been structurally characterized by single crystal X-ray study, which further enlightened the packing patterns of molecules in the solid state. The first report on exploitation of binuclear 1,1'-dithio complexes in thermochromism. The DMSO/DMF solution of **2** exhibit reversible charge transfer induced thermochromism in temperature range 30-90 ºC (DMSO) and 30-60 ºC (DMF). The enhanced cytotoxic activities of some of the the macrocyclic scaffolds **1-9** against human cancer HEP 3B and IMR 32 cells, as compared to cisplatin, a well known antineoplastic drug makes these compounds biologically significant.

3.1. Introduction

The dithiocarbamate ligands have been widely studies[1] in metal directed self-assembly, however, isostructural xanthate ligands have scarcely been investigated. Till date, literature evidences a single example of structurally characterized metallamacrocyclic complex based on xanthate ligand[2] and underlines their synthetic challenge, in spite of the ready availability of xanthate ligands bearing functionalized backbone. The current status of metal complexes derived from 1,1-dithio ligands in the literature and their potential needs in the area of metallopgarmaceticals is already highlighted in the introduction section of previous chapters.

Besides, synthetic degradable materials represented by aliphatic polyesters, particularly aliphatic polycarbonates (APCs) have been paid increasing attention in the vast field of biomedical and pharmaceutical sciences, due to their excellent physicochemical and mechanical properties.[3] Reportedly, functional groups on a polymer are usually responsible for material's biocompatibility and may tailor its macroscopic properties such as hydrophilicity/hydrophobicity, membrane permeability, bioadhesive ability, and biodegradability. Recently, 6,14-dimethyl-1,3,9,11-tetraoxa-6,14-diaza-cyclohexadecane-2,10-dione $(ADMC)_2$ has been emerged as a monomer to derived aliphatic polycarbonates. In this context, isostructural compounds of $(ADMC)_2$[4] could be of great interest. However, the number similar compounds are very limited due to elaborate synthetic procedures. There is an increasing need for new methods to construct such complex molecules, especially organic macrocyclic products with a variety of functionalities in backbone. Hence, the current synthetic strategy touching newer dimensions of metal complexes towards synthesis of organic macrocyclic scaffolds, those are enormously difficult to synthesize by conventional methodologies, would have great impact.

This section reports a facile one pot synthesis of metallamacrocyclic complexes $[M^{II}_2$-μ^2-bis-$\{(\kappa^2S,S\text{-}S_2COCH_2CH_2)_2N(R)\}]$ {R = Ts and M = Co^{II} **1**, Ni^{II} **2**, Cu^{II} **3**, Zn^{II} **4**; R = Bz and M = Co^{II} **5**, Ni^{II} **6**, Cu^{II} **7**, Zn^{II} **8**}. For the first time, we report the synthesis and structural characterization of a new functional organic macrocyclic compound **9**, 6,14-ditosyl-1,3,9,11-tetraoxa-6,14-diaza-cyclohexadecane-2,10-dithione containing tertiary amido groups in the backbone. All the compounds are characterized by relevant spectroscopic methods, microanalysis, theromgravometric study. Single crystal X-ray diffraction study has been performed

to elucidate the molecular structure and investigate packing pattern in solid state of some of the representative compounds. Moreover, thermochromism of compound **2** and potential *in vitro* cytotoxicity of $\mathbf{L^1}$-$\mathbf{L^2}$, **1-9** have been investigated.

3.2. Experimental

3.2.1. Synthesis of *N*-substituted diethanol amine precursors $\mathbf{L^1}$-$\mathbf{L^2}$

4-Toluenesulfonyl chloride (15.2 g, 79.89 mmol)/benzoyl chloride (11.2 g, 79.89 mmol) dissolved in dichloromethane (50 mL) was added drop wise to a solution of 2.5 equivalent of triethyl amine, 1 equivalent of diethanolamine (10 g, 95.1 mmol) over a period of 30 min at 0 ºC with stirring. During continued stirring for further 4 h, reaction mixture became viscous. Reaction progress was monitored with TLCs. After completion of reaction, excess 4-toluenesulfonyl chloride/benzoyl chloride was quenched by addition of distilled water. The product was extracted using dichloromethane and solvent was evaporated under vacuum. The crude product was purified: $\mathbf{L^1}$ by recrystallization (water:ethanol) and $\mathbf{L^2}$ by column chromatography (silica, ethyl acetate:hexane). The yields were were quantitative.

3.2.2. Synthesis of binuclear M^{II}xanthate macrocyclic complexes 1-8

In a typical procedure, ligand precursor $\mathbf{L^1}$ (259 mg, 1 mmol) or $\mathbf{L^2}$ (209 mg, 1 mmol) and KOH (123 mg, 2.2 mmol) were taken into a 100 mL single necked flask containing 20 mL CH_3CN solvent. To this mixture, an excess amount of carbon disulfide (0.5 mL, 10 mmol) was added with vigorous stirring. The reaction was allowed to continue for 12 h at room temperature. The formation of corresponding xanthate ligand was insured by a gradual consumption of diol precursor and a change in the colour from colourless to pale yellow. To this, corresponding metal acetate $Co^{II}(C_2H_3O_2)_2.4H_2O$ (249 mg, 1 mmol), $Ni^{II}(C_2H_3O_2)_2.4H_2O$ (249 mg, 1 mmol), $Cu^{II}(C_2H_3O_2)_2.H_2O$ (200 mg, 1 mmol) or $Zn^{II}(C_2H_3O_2)_2.2H_2O$ (220 mg, 1 mmol) was added with rigorous stirring and the reaction was allowed to continue further for 8 h at room temperature. The residue was isolated by filtration in a glass sintered crucible (**1-3** and **5-7**), or removing solvent under vacuum (**4** and **8**). Further, residues were washed for several times with acetonitrile followed by diethyl ether. Solid was dried under vacuum to yield the corresponding products **1-8** quantitatively. Products were stored under nitrogen atmosphere and samples were taken for analysis. The synthetic methodology is outlined in Scheme 1.

Table 1. Micro-, mass- and IR analysis data for compounds **L^1-L^2, K_2xan^1-K_2xan^1** and **1-8**.

Entry	Molecular Formula (MW)	Yield (%)	Mp (°C)	Elemental Analysis (%) Found (calculated)				IR data (KBr disk) υ_{max}/cm^{-1}
				C	H	N	S	
L^1	$C_{11}H_{17}NO_4S$ (259.32)	97	96.8	50.93 (50.95)	6.62 (6.61)	5.48 (5.40)	12.37 (12.36)	3250bs, 2970w, 2928w, 2881w, 2851w, 2721w, 1936w, 1598m, 1493m, 1470m, 1448m, 1375s, 1308s, 1289m, 1257w, 1162s, 1089s, 993s, 952s, 924m, 844m, 824s, 716s, 692s, 640m, 579w, 553s, 495w, 461w.
L^2	$C_{11}H_{15}NO_3$ (209.24)	89	296 b.p.	63.15 (63.14)	7.22 (7.23)	6.70 (6.69)	...	3390bs, 3063w, 3005w, 2948w, 2878w, 1720s, 1615s, 1602s, 1577m, 1499w, 1468m, 1422w, 1368w, 1314w, 1274s, 1178w, 1160w, 1116m, 1071s, 1027w, 1000w, 926w, 859w, 787w, 755s, 711s, 666w, 631w, 589w, 480s, 451m, 426m, 410s.
1	$C_{26}H_{30}Co_2N_2O_8S_{10}$ (937.04)	91	>149.2 dec.	33.35 (33.33)	3.22 (3.23)	3.00 (2.99)	34.27 (34.22)	2905w, 2834w, 1644m, 1574s, 1414s, 1380w, 1341m, 1220m, 1158m, 1112w, 1088w, 1019m, 922m, 813m, 736w, 712w, 658m, 619m, 548m, 465w, 437w.
2	$C_{26}H_{30}N_2Ni_2O_8S_{10}$ (936.56)	81	>182.2 dec.	33.35 (33.34)	3.24 (3.23)	2.99 (2.99)	34.25 (34.24)	2942w, 1915w, 1684w, 1596m, 1494w, 1461m, 1406m, 1374m, 1346m, 1330m, 1275s, 1235s, 1156s, 1137s, 1088s, 1043s, 1023s, 962w, 935s, 837w, 812m, 775m, 741s, 712w, 664s, 639m, 618w, 567m, 550s, 525m, 487w, 468m, 420w.
3	$C_{26}H_{30}Cu_2N_2O_8S_{10}$ (946.27)	89	>75.6 dec.	33.02 (33.00)	3.25 (3.20)	3.00 (2.96)	33.87 (33.89)	2886w, 2833w, 1754w, 1688w, 1568s, 1411s, 1379w, 1342m, 1200w, 1126s, 1089w, 1020m, 926m, 816w, 714w, 654m, 618s, 550m, 427w, 412w.
4	$C_{26}H_{30}N_2O_8S_{10}Zn_2$ (949.93)	73	>64.1 dec.	32.85 (32.87)	3.27 (3.18)	2.92 (2.95)	33.77 (33.75)	2883w, 1682s, 1662s, 1569s, 1554s, 1410s, 1220w, 1160w, 1089w, 1019m, 926m, 842m, 654m, 552w, 474w.
5	$C_{26}H_{26}Co_2N_2O_6S_8$ (836.88)	85	>167.2 dec.	37.35 (37.31)	3.12 (3.13)	3.34 (3.35)	30.67 (30.65)	2981w, 2929w, 2848w, 1719m, 1688w, 1610m, 1568m, 1550m, 1534m, 1419s, 1345m, 1274w, 1116s, 1012m, 952w, 936w, 802w, 712w, 685m, 665m, 619s, 544w, 493w.
6	$C_{26}H_{26}N_2Ni_2O_6S_8$ (836.40)	79	>75.9 dec.	37.37 (37.34)	3.12 (3.13)	3.33 (3.35)	30.34 (30.67)	2938w, 1975w, 1684m, 1574s, 1419s, 1348m, 1110w, 1049w, 1022m, 949w, 914m, 875w, 671s, 621w, 554w, 505w, 408w.
7	$C_{26}H_{26}Cu_2N_2O_6S_8$ (846.11)	80	>139.9 dec.	36.95 (36.91)	3.12 (3.10)	3.30 (3.31)	30.35 (30.32)	2990w, 2083w, 1722m, 1603s, 1447s, 1425s, 1318w, 1278m, 1121s, 1050m, 981w, 867w, 784w, 714m, 690m, 618s, 526w, 451w.
8	$C_{26}H_{26}N_2O_6S_8Zn_2$ (849.77)	65	>56.0 dec.	36.73 (36.75)	3.15 (3.08)	3.25 (3.30)	30.17 (30.19)	1734w, 1684m, 1570s, 1556s, 1408s, 1341m, 1152w, 1117w, 1049w, 1020m, 929w, 831w, 675m, 621w, 459w.
9	$C_{24}H_{30}N_2O_8S_4$ (602.76)	10		47.82 (47.82)	5.05 (5.02)	4.63 (4.65)	21.27 (21.28)	...

Table 2. NMR spectral data for compounds **L^1-L^2** and **$K_2(xan)^1$-$K_2(xan)^1$**.

Entry	NMR Data (ppm)	
	^{1}H NMR	**^{13}C NMR**
L^1 (CDCl3)	2.447 (s, 3H; C*H*$_3$), 3.269 (t, 4H; C*H*$_2$), 3.878 (t, 4H; C*H*$_2$), 4.838 (bs, 2H; O*H*), 7.340 (d, 2H; Ph), 7.710 (d, 2H; Ph).	21.53 (*C*H$_3$), 52.95, 62.05 (*C*H$_2$), 127.29, 129.89, 135.02, 143.80 (*C* of Ph). **DEPT-135**: δ (ppm) 21.54 (*CH*$_3$), 52.95, 62.06 (*CH*$_2$), 127.29, 129.90 (*CH* of Ph).
L^2 (CDCl3)	3.330 (d, 2H; C*H*$_2$), 3.530 (dd, 4H; C*H*$_2$), 3.750 (d, 2H; C*H*$_2$), 4.549 (bs, 2H; O*H*), 7.320 (m, 3H; Ph), 7.340 (m, 2H; Ph).	21.53 (*C*H$_3$), 49.42, 53.23, 60.00, 60.31 (*C*H$_2$), 127.07, 128.51, 129.61, 136.24 (*C* of Ph), 173.88 (CO). **DEPT-135**: δ (ppm) 49.41, 53.23, 59.83, 60.48 *(CH$_2$)*, 127.08, 128.52, 129.61 (*CH* of Ph).
4 (DMSO-d6)	1.708 (s; C*H*$_3$), 3.124 (t; C*H*$_2$), 3.493 (t, C*H*$_2$), 7.410 (m; Ph), 7.688 (m; Ph).	21.41 (*C*H$_3$), 51.52, 51.59, 59.96, 61.15, 60.36 (*C*H$_2$), 127.34, 127.46, 130.24, 130.28, 130.35, 136.52, 136.65, 143.48, 143.53 (*C* of Ph), 175.87 (-O^{13}CS$_2$).
8 (DMSO-d6)	1.718, 3.4 (bs; C*H*$_2$), 7.302, 7.877 (bs; Ph).	47.91, 52.02, 56.43, 58.92 (*C*H$_2$), 127.14, 127.73, 128.65, 129.30, 129.66, 137.65 (*C* of Ph), 171.52 (*C*O), 175.92 (-O^{13}CS$_2$).
9 (CDCl3)	1.257 (s, 3H; C*H*$_3$), 2.435 (s, 3H; C*H*$_3$), 3.255 (s, 4H; C*H*$_2$), 3.860 (s, 4H; C*H*$_2$), 7.327 (s, 2H; Ph), 7.695 (s, 2H; Ph).	21.53 (*C*H$_3$), 53.00, 62.23 (*C*H$_2$), 127.30, 129.87, 135.12, 143.77 (*C* of Ph), 173.31 (-CS). **DEPT-135:** δ (ppm) 21.54 (*CH$_3$*), 53.01, 62.23 (*CH$_2$*), 127.30, 129.88 (*CH* of Ph).

3.2.3. *In vitro* cytotoxic study

MTT assay for cell viability/ proliferation: The cell growth inhibition property for the investigated compounds against both the cell lines was determined by MTT assay with some modifications.[5] A series of binuclear M^{II}xanthate macrocyclic complexes **1-4**, **5**, **DEA**, **L^1-L^2**, corresponding metal acetates and Cisplatin were dissolved in DMSO and then diluted with water. The content of DMSO in the resultant solution for each sample was 1%. Cells were seeded in 96-well plates at a density of 1×10^3 cells per well followed by incubation for 24 h. The cells were treated with different concentrations of binuclear M^{II}xanthate macrocycles under investigation (entry 1-11) for 14 h against HEP 3B and IMR 32 cell lines. Thereafter, the media were removed and the culture was incubated with 20 μL of media containing 5 mg/ml stock solution of MTT in PBS and 60 μL of DMEM for 6 h at 37 °C in 5% CO_2 incubator. The metabolically viable cells leads to the formation of formazan crystals which further dissolved by adding DMSO. As the extent of formazan production is proportional to the number of viable cells, the formazan was estimated by the optical density measurement at 570 nm by ELISA reader (METERTECH-∑960).

3.3. Results and Discussion

3.3.1. Synthesis and Characterization

A series of binuclear M^{II}xanthate macrocyclic scaffolds of type $[M^{II}_2$-μ^2-bis-{(κ^2S,S-$S_2COCH_2CH_2)_2N(R)$}] **1-8**; where M^{II}: Co^{II}/ $Ni^{II/}$ Cu^{II}/ Zn^{II} and R: Ts/Bn, have been synthesized by the one-pot reaction protocol involving self-assembly of diol precursor *N*,*N*-Bis(2-hydroxyethyl)-4-methylbenzenesulfonamide (**L^1**) or *N*,*N*-Bis(2-hydroxyethyl) benzamide (**L^2**) with CS_2 and corresponding metal acetates in acetonitrile under basic condition. The one-pot synthetic methodology has been utilized extensively by Beer and coworkers to develop self-assembled transition metal based dithiocarbamate macrocycles.[1] Such a synthetic methodology involving several chemical operations simultaneously in a single vessel has some distinctive advantages, such as it can reduce the purifications of the intermediate compounds, predominantly important with unstable intermediates and may eventually save valuable resources.[6] The *in situ* formation of xanthate ligand is confirmed by the isolation and characterization of potassium salt of **L^1**, prepared adopting similar reaction condition.

Moreover, report[7] suggest that, dithiocarbamates of primary amine such as ethylenebis(dithiocarbamate) bearing flexible linker enabled intramolecular cyclization yielding ethylenethiourea derivatives under basic condition and in presence of Cu^{II} ions, however no reports are available till date on such type of reactivity of structurally similar xanthate compounds for synthesis of macrocyclic bis-(thiocarbonate O,O-ester). Interestingly, complex **4** showed the similar reactivity, yielding a 16 member macrocycle **9**. Macrocycle **9** is not formed in controlled reaction i.e. in absence of $Zn(OAc)_2$, however it can be formed (Yield: (10-12%) by rigorous stirring of complex **4** under mild basic condition in acetonitrile solution. Direct synthesis of such macrocyclic entity selectively by conventional methodologies is indeed extremely difficult, as it may suffer a number of side products and lack of stability of possible starting precursors (lack of suitable starting precursors). Hence, beside all these applications, the use of binuclear Zn^{II}xanthate macrocyclic scaffold **4** can be further extrapolated towards the effective synthesis of new organic macrocyclic scaffolds. The overall synthetic strategy is outlined in Scheme 1. In analogy with the recently reported 6,14-dimethyl-1,3,9,11-tetraoxa-6,14-diaza-cyclohexadecane-2,10-dione $(ADMC)_2$, macrocyclic compound **5,** 6,14-ditosyl-

1,3,9,11-tetraoxa-6,14-diaza-cyclohexadecane-2,10-dithione may be considered as a potential monomer for the development of functional polythiocarbonate based polymers with improved performance in the vast field of biomedical and pharmaceutical sciences,[3] compared to aliphatic polycarbonates (APCs).

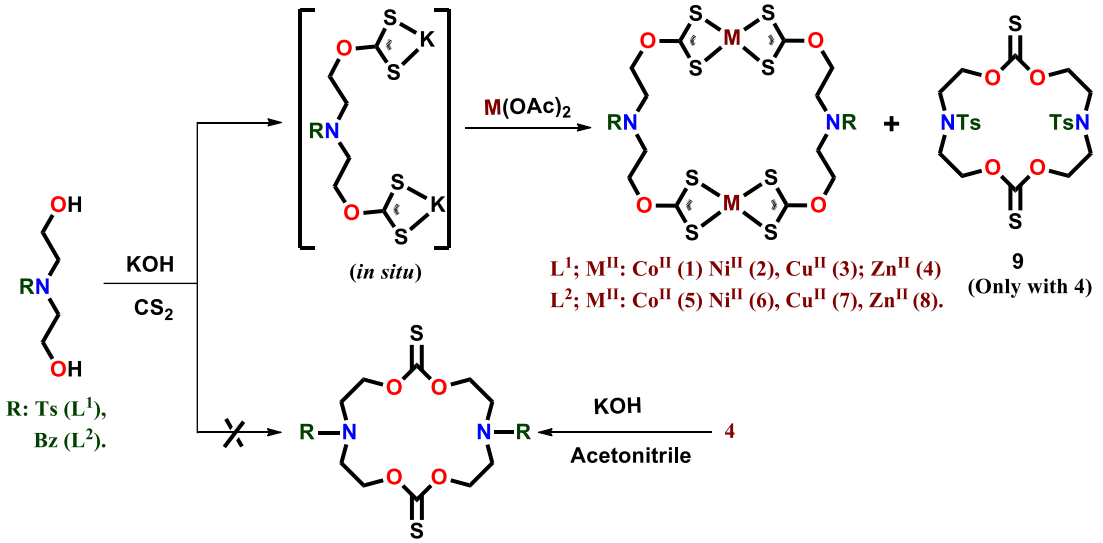

Scheme 1: General synthetic strategy for the synthesis of binuclear M^{II}xanthate macrocyclic complexes **1-8** and macrocycle **9**.

Although, the self-assembly of a discrete supramolecular structure always proceed in competition with polymerization,[8] literature reports underline its dependency on the stereo-electronic features of the ligand framework, nature of transition metal centres as well as thermodynamic conditions.[9] The formation of macrocycles is facilitated by the thermodynamic preference even if they are strained to some extent, profiting from enthalphic as well as entropic effects over oligomeric or polymeric species.

The isolated free flowing solids of binuclear M^{II}xanthate complexes (**1-3** and **5-7)** appeared to be air stable, while white colored binuclear Zn^{II}xanthate macrocycles (**2, 4**) are highly hygroscopic which immediately became sticky when exposed to air. The products are unstable on prolonged exposure to air; while in the solution state, they undergo decomposition over a period of time. Among the series of compounds, binuclear Ni^{II}xanthate macrocycle **2** and bis-(thiocarbonate O,O-ester) **9** were obtained in the crystalline state and their unambiguous structure was determined by single crystal X-ray analysis. However, rest of the compounds could not be obtained in the crystalline state, their composition and structures were elucidated by microanalysis, various spectroscopic data. To obtain further insights in the spectral data, geometry optimization of **1-9** were performed using DFT study. The elemental

analysis data for binuclear M^{II}xanthate macrocycles **1-8** and bis-(thiocarbonate O,O-ester) macrocycle **5** are in good agreement with their compositions as per the proposed chemical formula which is mutually supported by subsequent spectroscopic data and thereafter theoretical studies. The characterization data for **1-9** is summarized in the experimental section.

In the IR spectra of complexes **1-8,** the absence of ν(O-H) vibration bands (3390-3250 cm^{-1}) and appearance of new bands in the regions 1160-1018 cm^{-1} as the characteristic of the xanthate moiety clearly suggest the formation of desired macrocycle. Reports suggest that the IR bands in [$ROCS_2$] groups are highly coupled and exhibit four characteristic bands around 1250 cm^{-1}, 1100 cm^{-1}, 1020 cm^{-1}, and 550 cm^{-1} attributable to ν(C=S), ν(C-O), ν(C-S), and ν(R-O) vibrations.[10] According to Bonati and Ugo,[11] the presence of only one strong band in the region 950-1050 cm^{-1} is assumed to indicate a isobidentate bonding of the 1,1-dithio ligands to the metal centre, while a split band is an indicative of asymmetrically bound bidentate ligand. The presence of only one band in the region of 950-1050 cm^{-1} of the ν(CSS) vibration, suggests a symmetrical behavior of the bidentate xanthate moiety, which is further reinforced by optimized geometries by DFT study. Notably a strong band at ~ 925 cm^{-1} appeared in $\mathbf{L^1}$ and **1-4** are mainly due to the aromatic ν(C-H) out-of plane bending vibrations, a characteristic feature of para-disubstituted benzene rings.[12] For $\mathbf{L^2}$ and **5-8**, a characteristic aromatic ν(C-H) out-of plane bending vibrations of monosubstituted benzene rings are mainly appeared at 670-870 cm^{-1}. The ν(M-S) bands greatly depends on the nature of the metal ion and the ancillary part of ligand. In agreement with the observations made by Watt and McCormick, we have observed medium to weak intensity ν(M-S) bands in the 675-545 cm^{-1} range.

The ^{1}H and ^{13}C spectral study clearly supports the formation of binuclear Zn^{II}xanthate complexes and conformational mobility within the macrocyclic assembly. A significant shifting of the *N*-methylene signals of the complexes, compared to free diol precursors reinforce the formation of proposed structures as they are most sensitive to any kind of chemical change at –OH functionality. The binuclear M^{II}xanthate macrocycles **4** and **8** display a downfield resonance at 175.87 and 175.92 ppm, characteristic of coordinated xanthate (-$O^{13}CSS$) moiety.[12] Despite of diamagnetic nature of Ni^{II}xanthate complex **2** in solid state, we could not detect good ^{1}H and ^{13}C NMR signals for complexes **2** and **6** mainly due to their unique

behaviour in solution; as Ni^{II} centres adopt octahedral geometry in solution (especially DMF/DMSO) and the resultant complex display paramagnetic nature. Moreover, bis-(thiocarbonate O,O-ester) macrocycle **9** display ^{13}C signals at 21.54, 53-63, 127-144 and 173.31 ppm due to $–CH_3$, $-CH_2$, aromatic and -C=S carbons respectively, which is consistent with DEPT-135 spectrum.

3.3.2. UV-visible absorption and Emission Property

The UV-visible absorption and emission spectra of ligand precursors **L^1**, **L^2** and binuclear M^{II}xanthate complexes **1-8** were measured at room temperature from 10^{-4} M DMSO solution samples. The UV-visible absorption spectra are shown in Figure 1 and the subsequent results are summarized in Table 1.

Table 1. UV–visible absorption and emission spectra data for ligand precursors **L^1-L^2** and binuclear M^{II}xanthate complexes **1-8**.

Entry	UV-visible spectral data λ_{max} nm; (Absorbance)	Emission spectral data λ_{em} nm; (Intensity a.u.)	λ_{ex} nm
	DMSO solution		
L	262 (0.1067)	287 (64)	262
L^1	264 (1.7262)	291 (89)	264
L^2	276 (2.6094)	358 (221), 426 (239)	276
K-xanL^1	279sh (3.2726), 300 (3.4302), 346 (2.9041), 365sh (2.5355).	417 (12), 472 (29), 492 (32), 538 (14)	300
1	234 (0.8941), 259sh (1.6535), 284 (2.0029), 360 (1.1934), 514 (0.5443), 574 (0.5246)	408 (30), 437 (38)	360
2	282 (3.0839), 315 (3.3108), 354 (2.4139), 678 (0.0752)	467 (9), 498 (6)	315
3	276 (2.8364), 319 (3.0776), 335sh (2.0207), 714 (0.0517)	354 (68), 418 (75), 467 (73)	276
4	273 (3.035), 289sh (2.0071), 375sh (0.6266)	330 (233), 418 (337)	274
5	246 (0.4933), 264 (0.9105), 331sh (0.3802), 526 (0.2326), 573 (0.2527)	369 (171), 411(151)	331
6	263 (0.5503), 319 (0.2770), 405 (0.1134), 722 (0.0241), 786 (0.0271)	287 (32), 355 (176)	263
7	285 (3.3854), 370 (0.8116), 716 (0.3609)	342 (62), 435 (139)	285
8	265 (1.7772), 294 (1.4640)	330 (221), 422 (578)	265
	CH_2Cl_2 solution		
2	313 (4.018), 326 (4.724), 335sh (3.086), 426 (2.041), 502 (1.9065)	….	…
2+DMF	313 (1.713), 426 (0.191), 492 (0.130), 698 (0.048)	….	…
6	329 (0.188), 394 (0.049), 439 (0.019), 524 (0.009)	….	…

The assignments of UV-visible absorption and emission bands are based on the literature reports on closely related compounds.[13] The ligand precursors **L^1-L^2** exhibit a single prominent band at shorter wavelength 264-276 nm, attributable to π→π* (phenyl) transitions additionally the difference in λ_{max} values reflects the effect of change in the *N*-substituents. All binuclear complexes **1-8** display three principal bands at ~250 nm, ~ 300 nm and at ~ 350 nm, attributable to π→π* (phenyl), n→π*

and charge transfer transitions, respectively, which is consistent with the absorption behavior of transition metal xanthate complexes.[13] Further, characteristic d-d transition bands are indicative of the corresponding coordination sphere *ca.* tetrahedral/square planar and octahedral geometry is adopted by Co^{II}/Cu^{II} and Ni^{II} centres, respectively in solution state. Notably, UV-visible absorbance spectra of binuclear Ni^{II}xanthate complexes **2** and **5** in CH_2Cl_2 solution displayed absence of bands at ~ 680 nm, indicative of square planar coordination geometry around Ni^{II} centre similar to the X-ray structure of **2**. However, addition of small amount of DMF in CH_2Cl_2 solution of **2** resulted into the occurrence of characteristic d-d transition bands at 698 nm, which suggest the change in the coordination geometry around Ni^{II} centre from square planar to octahedral, as that of samples analysed in DMSO solution.

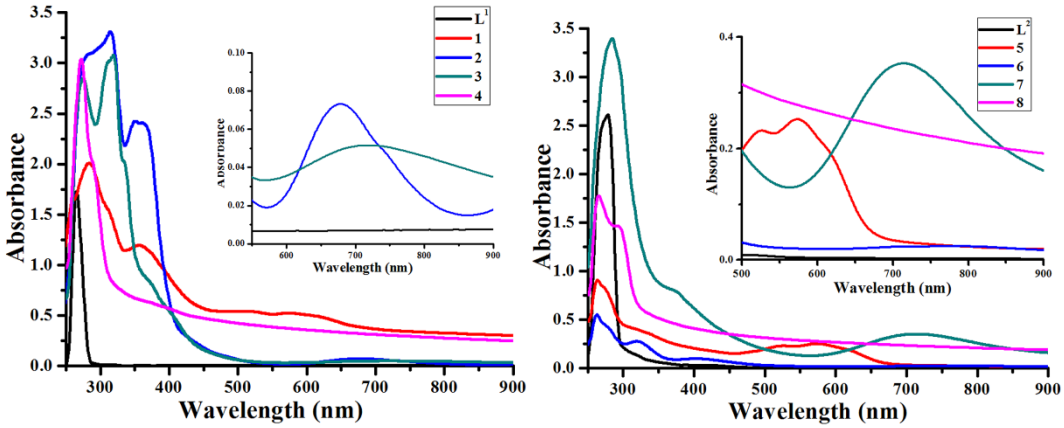

(a) (b)

Figure 1. UV-visible absorption spectra for **L^1, 1-4** (a) and **L^2, 5-8** (b) in 10^{-4} M DMSO solution.

On the other hand, fluorescence study evidently depicted the significant quenching of the fluorescence property of binuclear M^{II}xanthate macrocyclic complexes **1-8 (**except **4** and **8)**, compared to their respective ligand precursors **L^1** and **L^2**. All the complexes **1-8** exhibit maximum fluorescence emissions at 426, 437, 466, 418, 369, 355, 435 and 422 nm upon excitation at 360, 315, 276, 274, 331, 260, 285 and 265 nm with concomitant Stokes shifts of 66, 122, 190, 144, 38, 95, 150 and 157 nm, respectively. (Figure 2) Notably, among all the binuclear M^{II}xanthate macrocycles, complex **4** and **8** bearing Zn^{II} centre exhibit the maximum fluorescence property which may be attributed to the reduction of photoinduced electron transfer process on complex formation.[14] The emission spectra of majority of the complexes displayed similar patterns, i.e. two or more kinds of fluorescence emission bands are appearing by the excitation of single absorption bands (in any case, shoulder is

appearing). Such a trend of fluorescence spectra and concomitant bathochromic shifts of intramolecular charge-transfer emissions is consistent with previous reports on transition metal xanthate complexes.[13] It appears from the literature that the photoinduced electron transfer processes, hence fluorescence properties of the compounds is greatly affected by the molecular arrangements, conformational stiffness of the fluorophore (dihedral angles), non-covalent interactions and the nature of substituents.[15]

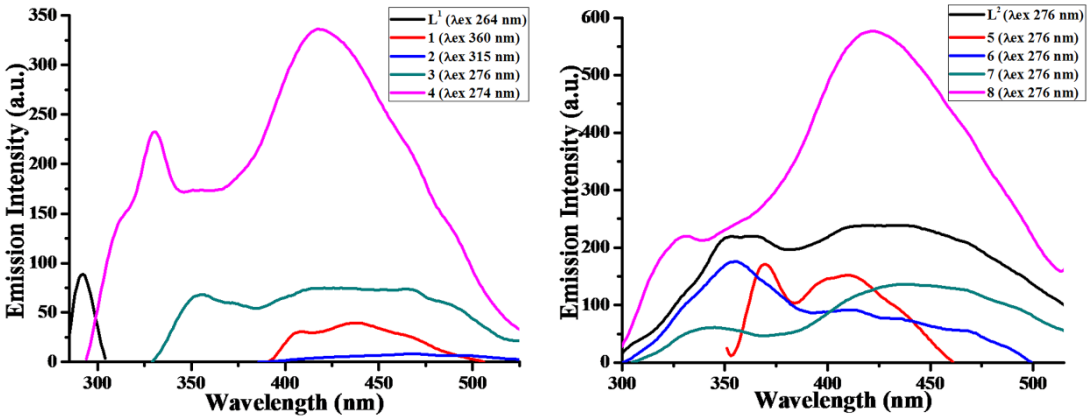

(a) (b)

Figure 2. Fluorescence spectra for **L^1, 1-4** (a) and **L^2, 5-8** (b) in 10^{-4} M DMSO solution.

3.3.3. Thermochromic behavior of binuclear Ni^{II}xanthate complex 2

In the light of thermochromism ability of Ni^{II} complexes bearing sulfur donor ligands,[16] binuclear Ni^{II}xanthate complexes **2** and **6** were investigated for their potential thermochromic behaviour. The DMSO/DMF (1.5×10^{-3} M) solution of the binuclear Ni^{II}xanthate macrocycle manifests a reversible colour change for the temperature range of 30–90 ºC (for DMSO) and 30–60 ºC (for DMF) as illustrated in Figure 3-6. The solution is green coloured at low temperature, where the Ni^{II} hexacoordinated with the two solvent ligands. With increase in the temperature of DMSO solution of **2**, the green coloured solution gradually turns to brownish colour, a significant change in colour is noted at 80-85 ºC. This can also be visualized with gradual change in UV-visible absorption spectrum, especially at 55 ºC a new charge transfer band appears at λ_{max} 478 nm ($\varepsilon \approx 154$ dm^3mol^{-1} cm^{-1}) which on further increase of temperature at 60 ºC got enlarged with slight red shift (λ_{max} 478, $\varepsilon \approx 200$ dm^3mol^{-1} cm^{-1}) (Figure 4) with colour change green to pale yellowish brown. However, increased temperature of DMF solution of **2** lead to colour change from green to brownish colour, a significant change in colour is noted at 50-55 ºC, which is

significantly lower than that of DMSO solution (-30 ºC). This colour change is well accompanied with gradual change in UV-visible absorption spectrum especially a charge transfer band at 397-411 nm. It appears that at lower temperature i.e. 30-40 ºC a band at λ_{max} 397 nm diminishes with new band at λ_{max} 407 nm ($\varepsilon \approx 996$ dm^3mol^{-1} cm^{-1}) which on further increase of temperature got enlarged with significant red shift (at 60 ºC λ_{max} 411, $\varepsilon \approx 1482$ dm^3mol^{-1} cm^{-1}) (Figure 6). Further, for another charge transfer band at λ_{max} 480 nm, no significant shift could be observed, instead significant change in absorbance is noted. Literature reports depicted the thermochromic nature of mononuclear Ni^{II} complexes bearing S donor ligands achieved through reversible ligand-exchange and change in coordination geometry.[16] Almost unchanged (i.e. absence of any shift) d-d transition bands in respective solvent systems with change in the temperature ruled out the possibility of thermochromic nature achieved through reversible ligand-exchange and change in coordination geometry for investigated system, unlike reports on square planar NiS4 complexes.[16] A point to be noted that a further increase in temperature till 110 ºC lead to the intense colour change, but it is irreversible. Hence, the complex **2** displays charge transfer based thermochromic behavior in the 30–90 ºC (for DMSO) and 30–60 ºC (for DMF) range. Although very few reports illustrate this phenomenon in transition metal complexes, no reports are available on any of the xanthate complex as well as binuclear M^{II}(1,1-dithio) macrocyclic complex as per the best of our knowledge.

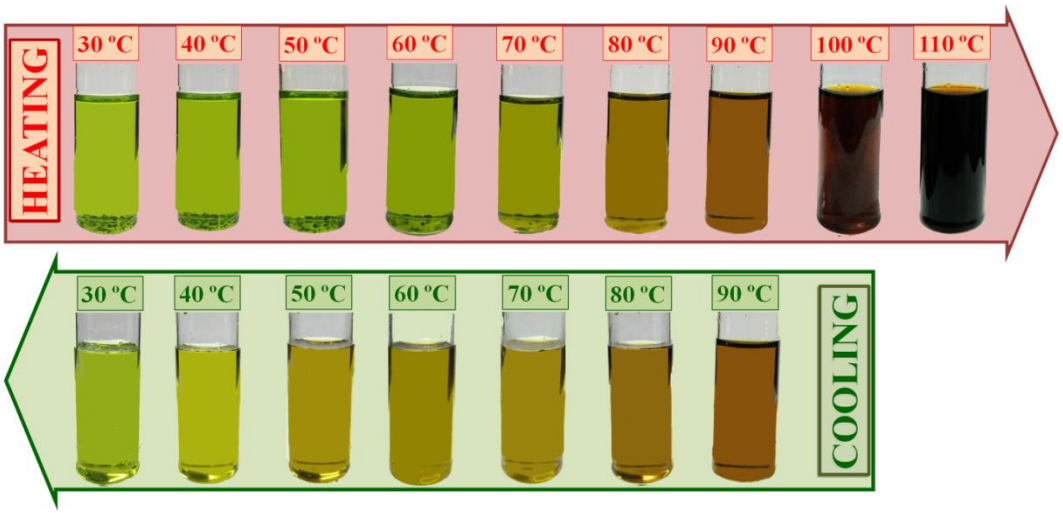

Figure 3. Color change from green to brown of DMSO solution of **2** (1.5×10^{-3} M) in temperature range 30-110 ºC.

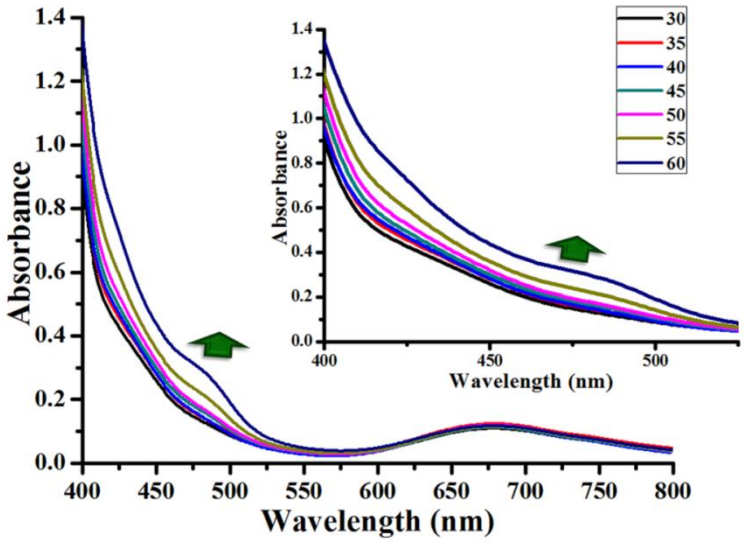

Figure 4. UV-visible spectrum of **2** in DMSO solution (1.5×10^{-3} M) recorded at temperature range 30-60 ºC.

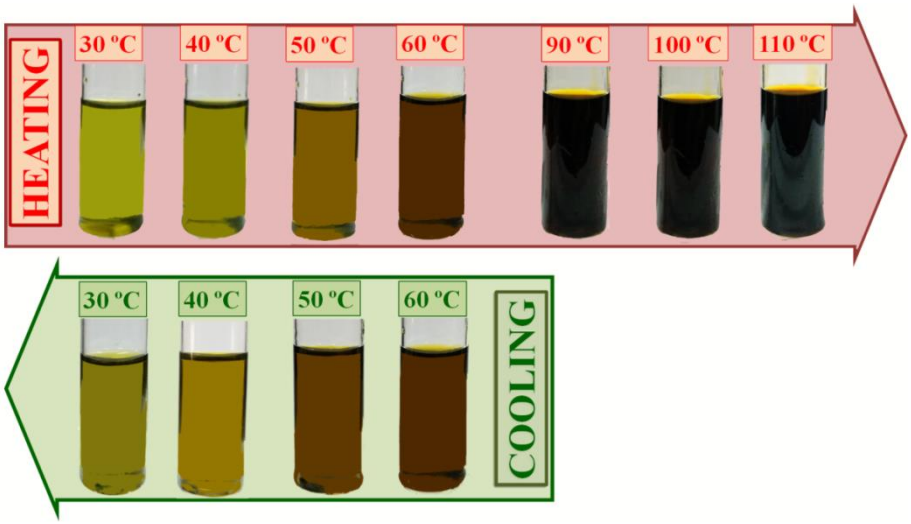

Figure 5. Color change from green to brown of DMF solution of **2** in temperature range 30-110 ºC.

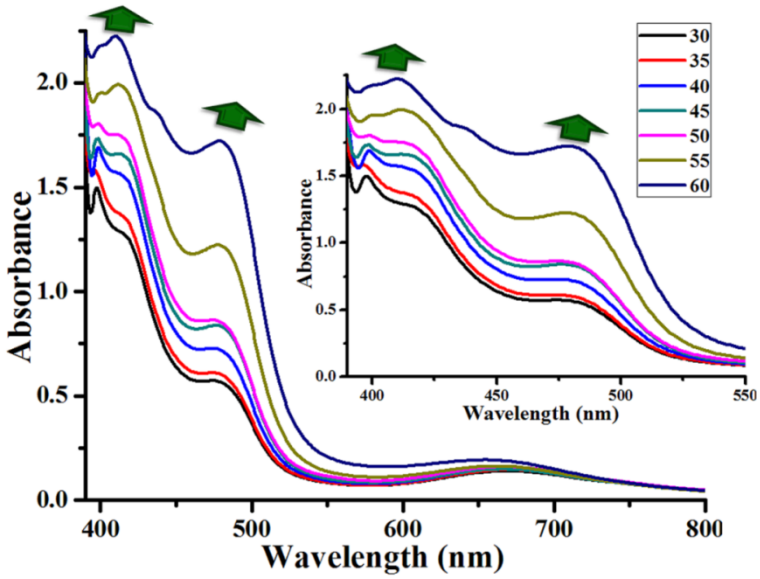

Figure 6. UV-visible spectrum of **2** in DMF solution (1.5×10^{-3} M) recorded at temperature range 30-60 ºC.

3.3.4. Thermogravimetric Study

All the diol precursors **L^1-L^2** and binuclear M^{II}xanthate macrocycles **1-8** were studied for their thermal behavior. The thermogravimetric study for **L^1-L^2** and **1-8** was performed at a heating rate of 10 °C /min under N_2 atmosphere from room temperature to 550 °C. The TGA/DTA plots are given in annexure, thermal analysis data and corresponding TG curves are given in Table 2 and Figure 7, respectively.

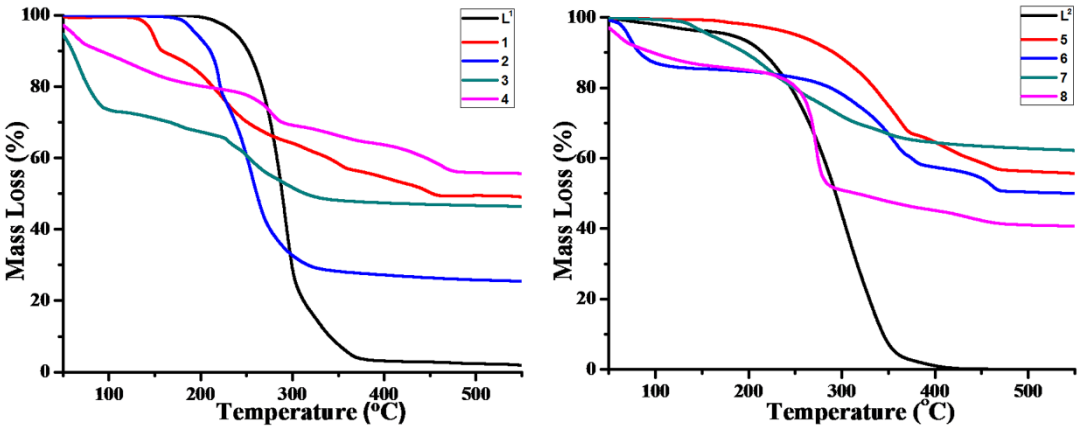

(a) (b)

Figure 7. TG curves for **L^1, 1-4** (a) and **L^2, 5-8** (b).

A single step mass loss of the diol precursors and multistage thermal degradation was observed on corresponding TG curves (Figure 7) which are indeed accompanied by various endothermic and/or exothermic peaks DTA curves (Annexure). For both the ligand precursors **L^1** and **L^2** maximum rate of mass loss observed at 287.4 °C and 296.0 °C mainly due to evaporation with complete mass loss till 550°C. Different temperatures corresponding to the maximum rate of mass loss of **L^1-L^2** and complexes **1-6** were recorded on DTG curves. Notably, all the xanthate complexes **1-8** showed a multistage thermal degradation pattern due to the elimination of different molecular fragments, evidence by TG curves (Figure 7) which are indeed accompanied by corresponding peaks on DTG curves. On the other hand TG curves demonstrate relatively greater thermal stability of binuclear M^{II}xanthate macrocycles **2** than others. Although, the thermal degradation of all the complexes is continued at 550 °C, however, Ni^{II} complexes **2** gave a stable residual mass of 25.7 % which may correspond to NiS (calc. 19.4 %) plus small amount of char. Reportedly the size and shape of the metal sulfide nanoparticles greatly depend on the nature of organic moiety present in metal 1,1-dithio complexes[17] which consecutively affect the fundamental properties like optical, electrical and mechanical properties.[18] The thermogravimetric analysis indicates the suitability complexes **2** as single source

precursors for the synthesis of Nickel Sulphide nano particles and thin films[19] which adds further merit to this class of compounds.

3.3.5. Structural Details

X-ray crystallography and data collection: Crystals of binuclear Ni^{II}xanthate complex **2** and bis-(thiocarbonate O,O-ester) macrocycle **9** suitable for X-ray crystallographic study was obtained in acetonitrile by slow evaporation at room temperature and in diethyl ether at 4 ºC, respectively. Intensity data were collected on 'Xcalibur, Eos, Gemini' X-ray diffractometer equipped with Eos CCD detector at 293 K for [$C_{26}H_{30}N_2Ni_2O_8S_{10}$] **2** and [$C_{24}H_{32}N_2O_8S_4$] **9**. Monochromatic CuKα X-ray (λ = 1.54184 Å) radiation was used for the measurements. Data were collected and CrysAlisPro data reduction: Agilent Technologies Version 1.171.36.28 program(s) used to process the data.[20] The crystal structures were solved by direct methods and the refinement was carried out against F^2 using SHELXL-97 program package.[21] All non-hydrogen atoms were refined anisotropically. The crystal data and structure refinement for **2** and **9** are given in Table 2.

Table 2. Crystal data and structure refinement for compounds **2** and **9**.

Compound	**2**	**9**
Formula	$C_{26}H_{30}N_2Ni_2O_8S_{10}$	$C_{24}H_{30}N_2O_8S_4$
Formula weight(amu)	936.60	602.74
Temperature (K)	293(2)	293 (2)
Crystal System	monoclinic	triclinic
Space group	$P2_1/n$	P-1
a(Å)	9.8676(3)	6.0869(3)
b(Å)	5.69613(14)	7.5178(5)
c(Å)	33.5649(10)	16.0444(10)
α(°)	90.00	84.939(5)
β(°)	97.591(3)	87.956(5)
γ(°)	90.00	70.805(5)
Cell volume ($Å^3$)	1870.06(10)	690.66(7)
Z	2	1
Completeness to theta (%)	(θ = 66.97) 98.41	(θ = 66.97) 99.68
$\rho_{calc}g/cm^3$	1.663	1.449
μ/mm^{-1}	6.883	3.596
F(000)	960.0	316.0
Radiation	CuKα (λ = 1.54184)	CuKα (λ = 1.54184)
2θ range for data collection/°	10.64 to 133.12	11.08 to 143.88
Index ranges	$-10 \le h \le 11, -4 \le k \le 6, -39 \le l \le 39$	$-6 \le h \le 7, -8 \le k \le 9, -18 \le l \le 19$
Reflections collected	9490	4434
Independent reflections	3302 [R_{int} = 0.0267, R_{sigma} = 0.0282]	2723 [R_{int} = 0.0236, R_{sigma} = 0.0341]
Data/restraints/parameters	3302/2/217	2723/0/173
Goodness-of-fit on F^2	1.023	1.063
Final R indices [I>2σ(I)]	R_1 = 0.0361, wR_2 = 0.0901	R_1 = 0.0690, wR_2 = 0.2025
R indices (all data)	R_1 = 0.0477, wR_2 = 0.0971	R_1 = 0.0743, wR_2 = 0.2079
Largest diff. peak/hole / e $Å^{-3}$	0.38/-0.20	0.79/-0.59

Table 3. The selected bond distance (Å) and bond angle (°) for **2** and **9** are:

Selected Atoms	Bond Distance (Å)	Selected Atoms	Bond angle (°)
	2		
Ni4-S1	2.2022(9)	S1-Ni4-S2	79.37(3)
Ni4-S2	2.2217(9)	S12-Ni4-S22	79.75(3)
Ni4-S12	2.2144(10)	S1-Ni4-S12	177.38(4)
Ni4-S22	2.1930(9)	S2-Ni4-S22	177.86(4)
C47-S1	1.692(3)	S1-C47-S2	113.46(17)
C47-S2	1.687(3)	S12-C37-S22	113.52(17)
C37-S12	1.692(3)	C47-O5-C65	119.5(2)
C37-S22	1.686(3)	C72-O15-C37	118.3(2)
C47-O5	1.301(4)		
C37-O15	1.304(4)		
C65-O5	1.463(3)		
C72-O15	1.458(3)		
	9		
S3-C6AA	1.654(4)	S3-C6AA-O2	127.6(3)
O2-C6AA	1.326(4)	S3-C6AA-O3	126.8(2)
O3-C6AA	1.331(4)	O2-C6AA-O3	105.6(3)
O3-C5AA	1.444(4)	C4AA-O2-C6AA	119.5(3)
O2-C4AA	1.464(4)	C5AA-O3-C6AA	116.0(3)

Structural descriptions: Both of these binuclear Ni^{II}xanthate complex **2** and bis-(thiocarbonate O,O-ester) macrocycle **9** are composed of three types of molecular subunits, viz. sulfur atoms, *N*-Ts substituent and alkyl chain linker. Alkyl linker is essential to afford the flexibility by bending the molecule so as to it could capable to form macrocyclic architectures. The *N*-Ts substituent and sulfur atoms present in molecular framework changes the electronic nature across the molecules and potentially provide a sites for noncovalent interactions like CH...π, CH...O and CH...S intermolecular interactions. Mutually all the noncovalent interactions lead to the formation of double helical molecular self-assembly.

Binuclear Ni^{II}xanthate complex 2: Compound **2** crystallizes in centrosymmetric monoclinic $P2_1/n$ space group. The X-ray crystal structure of **2** show a half of the molecule of $[C_{26}H_{30}N_2Ni_2O_8S_{10}]$ in its asymmetric unit and complete molecule is generated through symmetry operation [2-X, 1-Y, 1-Z] which lies on a centre of inversion, is shown in Figure 8(a). The crystal structure showed the disordered *N*-tosyl substituent, occupancy is assigned to 0.329(17) : 0.671(17). Such six units are present in the unit cell. For macrocycle **2**, Ni-S bond distances (2.1930-2.2217 Å), S-Ni-$S_{(chelate)}$ (79.37-79.75 °) and S-Ni-$S_{(trans)}$ (177.38-177.86 °) bond angles clearly suggest presence of square planar NiS_4 coordination sphere, also underlines the symmetrical binding of xanthate ligands. These structural parameters are significantly smaller than similar type of binuclear xanthate macrocyclic crown ether[2] bearing anisobidentate xanthate ligands coordinate in planar NiS_4 coordination sphere (Ni-S

bond distances: 2.2098-2.2285 Å, S-Ni-$S_{(chelate)}$: 79.45-102.07 ° and S-Ni-$S_{(trans)}$: 177.06-178.52 °). The X-ray structure clearly depicted the formation of macrocycle with cavity size ~ 13.03 × 4.28 $Å^2$ with 4.286 Å transannular Ni-Ni distance. The relevant parameters, selected bond distance (Å) and bond angle (°) for **2** are tabulated in Table 3.

In the crystal packing, each molecule forms nine molecules supramolecular aggregate through number of CH...π, CH...O, CH...S, S...O and S...S donor-acceptor interactions which is extended to the 3D infinite assembly, as shown in Figure 8(b). The details about non-covalent interactions like interatomic distances (Å), bond angles (°) are summarized in table 2. Of more interesting, the **H39B...π** interactions lead to the 1D infinite packing of molecules in wavy fashion in *ac*-plane as shown in Figure 8. The **H26A...O** interactions are closing contact and indeed associated with CH...S, S...S interactions forming macrocyclic assembly, mutually these contacts forms an attractive 1D infinite ladder like as assembly along *b*-axis. (Figure 8) Further, **H72A...S** interactions packed molecules parallel in *ac*-plane forming ladder like assembly. Notably, unlike to binuclear xanthate macrocyclic crown ether[2] no Ni...S interactions are observed. All these noncovalent interactions present in complex **2** mutually resulting into the formation of 3D infinite supramolecular assembly.

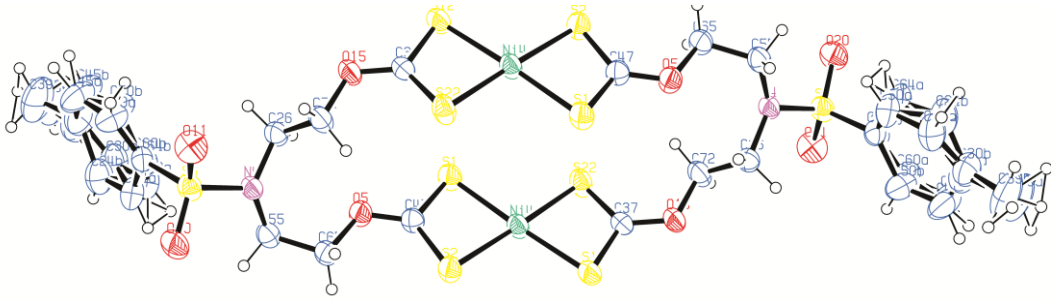

(a)

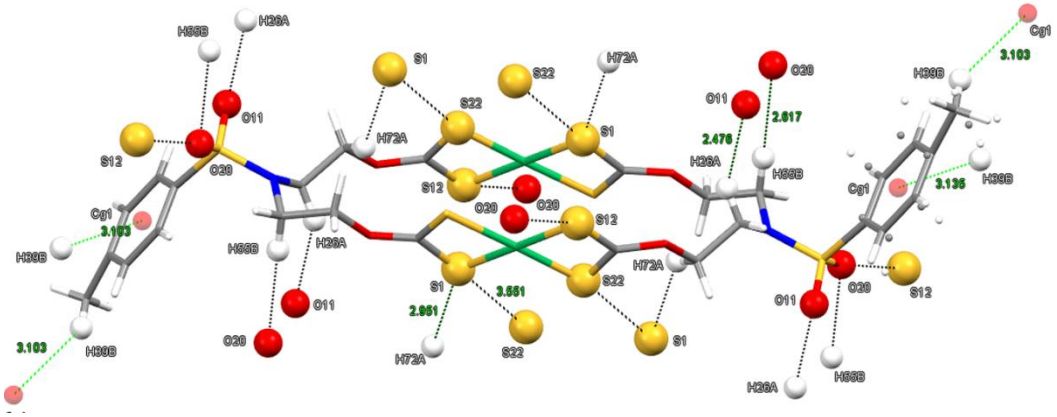

(b)

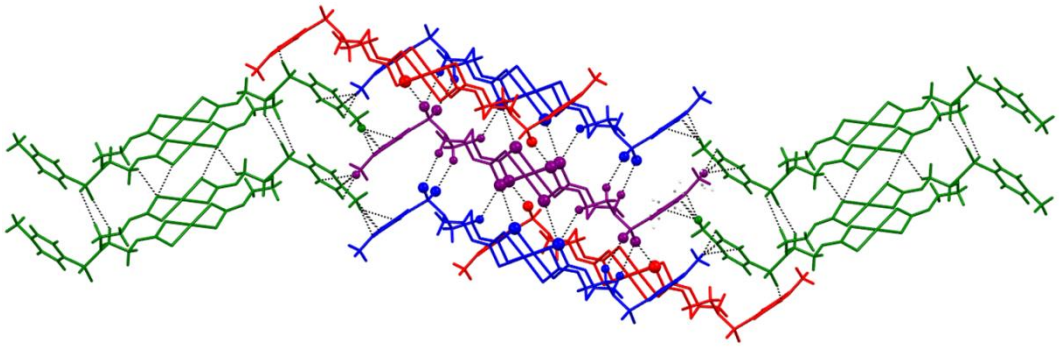

(c)

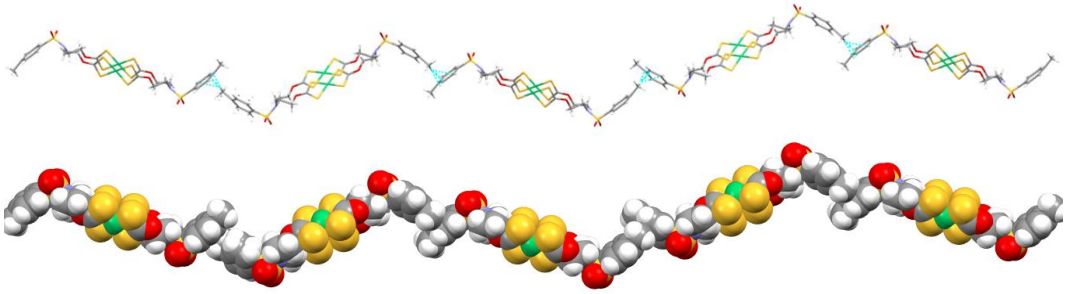

(d)

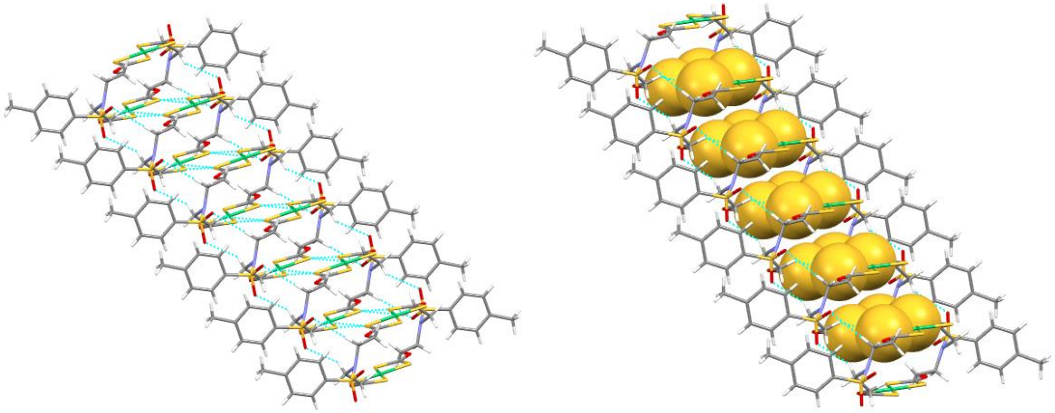

(e)

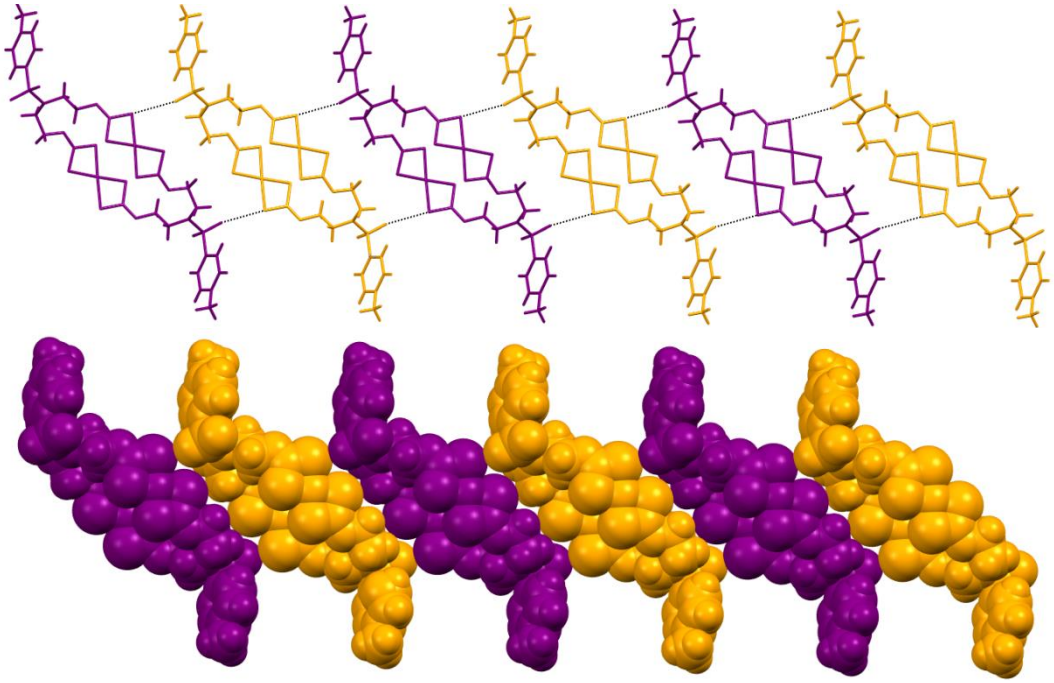

(f)

Figure 8. (a) An ORTEP view of **2** at 40% probability, (b) noncovalent interaction present in **2**, (c) supramolecular aggregate formed through intermolecular weak interactions, (d) 1D wavy packing of **2**, (e) CH...O, CH...S interactions mutually leading to an attractive 1D infinite ladder like as assembly along *b*-axis, (f) 1D molecular stacking consisting '*S*' shaped molecules through CH...S closing interactions.

Table 4. Significant intermolecular interactions [Interatomic distances (Å), and bond angles (°)] found in compounds **2** and **9**.

Interactions	D─H…A	D─H	H…A	D…A	<DHA
		2			
CH…π	C_{39}─H_{39B}…C_{g1}	0.957	3.103	3.969	151.17
CH…O	C_{26}─H_{26A}…O_{11}	0.971	2.476	3.284	140.49
	C_{45}─H_{45B}…O_{11}	0.930	2.475	3.323	151.63
	C_{55}─H_{55B}…O_{20}	0.970	2.617	3.587	179.11
CH…S	C_{72}─H_{72A}…S_1	0.970	2.951	3.703	135.20
S…O	O_{20}…S_{12}	-	-	3.114	-
S…S	S_1…S_{22}	-	-	3.551	-
		9			
CH…π	C_{13}─H_{13C}…C_{g1}	0.959	2.916	3.746	145.49
CH…O	C_{10}─H_{10}…O_4	0.930	2.468	3.299	148.81
	C_{7AA}─H_{7AB}…O_1	0.970	2.468	3.327	147.55
CH…S	C_8─H_{8AA}…S_3	0.970	2.921	3.738	142.55
O…O	O_2…O_2	-	-	3.005	-

Bis-(thiocarbonate O,O-ester) macrocycle 9: Compound **9** crystallizes in centrosymmetric triclinic *P*-1 space group. The X-ray crystal structure of **9** show a half of the molecule of [$C_{24}H_{32}N_2O_8S_4$] in its asymmetric unit and complete molecule is generated through symmetry operation [2-X,-Y,-Z] which lies on a centre of inversion, is shown in Figure 9(a). Such eight units are present in the unit cell. The

relevant structural parameters are tabulated in Table 2. In the crystal packing, each molecule forms seven molecules supramolecular aggregate through number of CH...π, CH...O, CH...S and O...O donor-acceptor interactions which is extended to the 3D infinite assembly, as shown in Figure 9(b). The details about non-covalent interactions like interatomic distances (Å), bond angles (°) are summarized in table 2. Of more interesting, the **CH...O** interactions are associated with **CH..S** interactions lead to the 1D infinite network in *ab*-plane, whereas **CH…π** interactions stack molecules along *c*-axis. These noncovalent interactions present in complex **9** mutually resulting into the formation of 3D infinite supramolecular assembly consisting molecular cavities of dimensions ~ 6.60 × 3.47 $Å^2$.

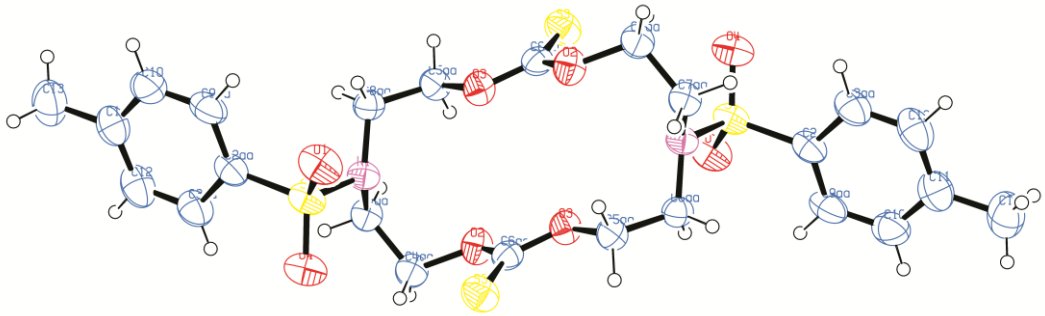

(a)

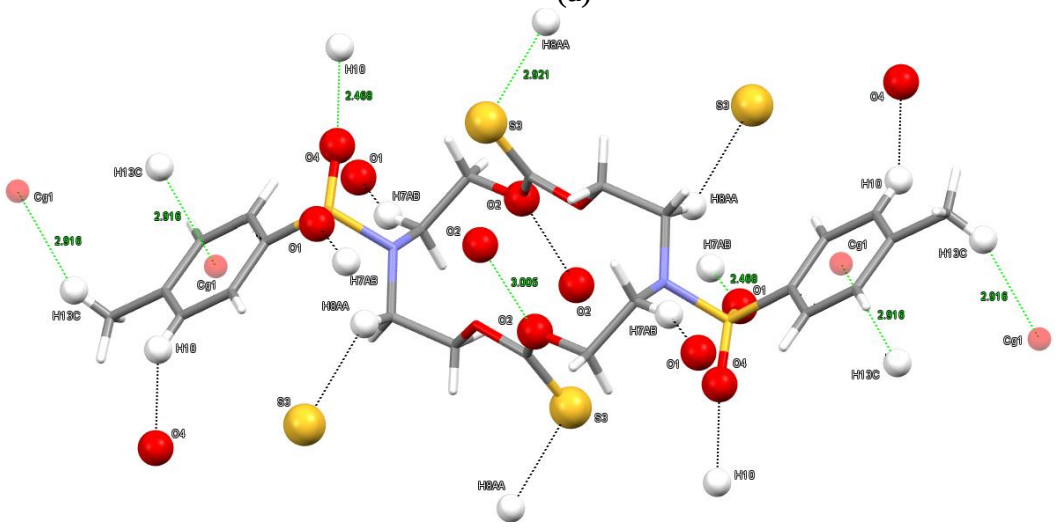

(b)

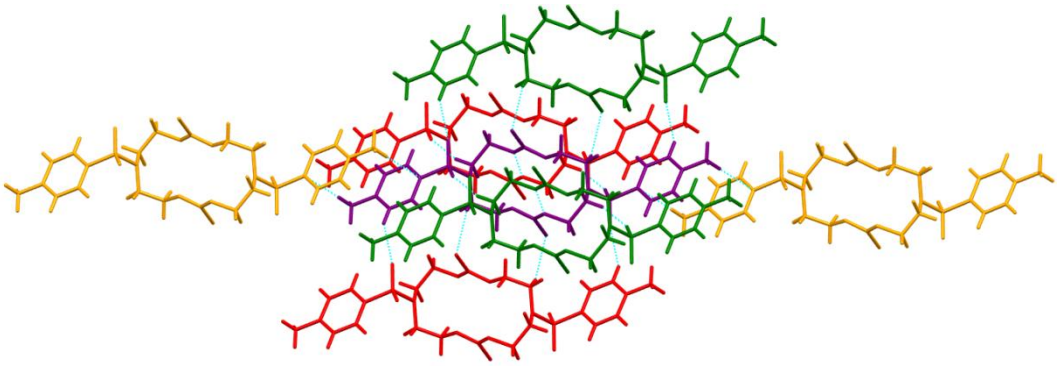

(c)

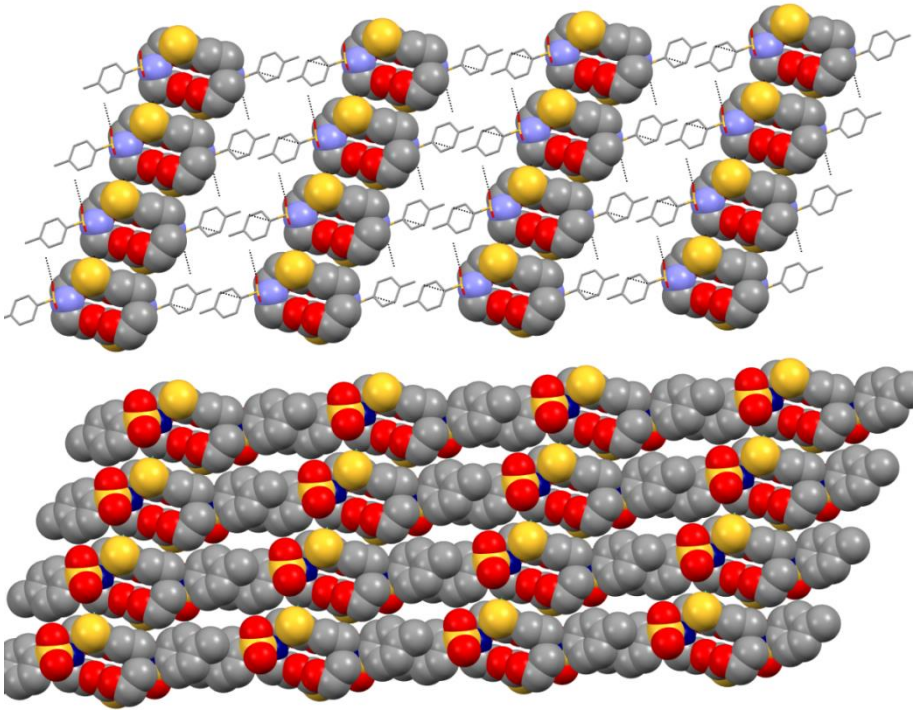

(d)

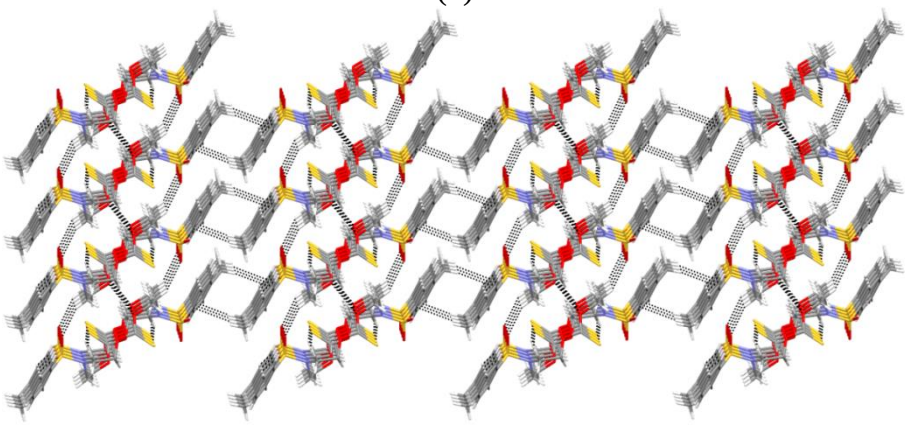

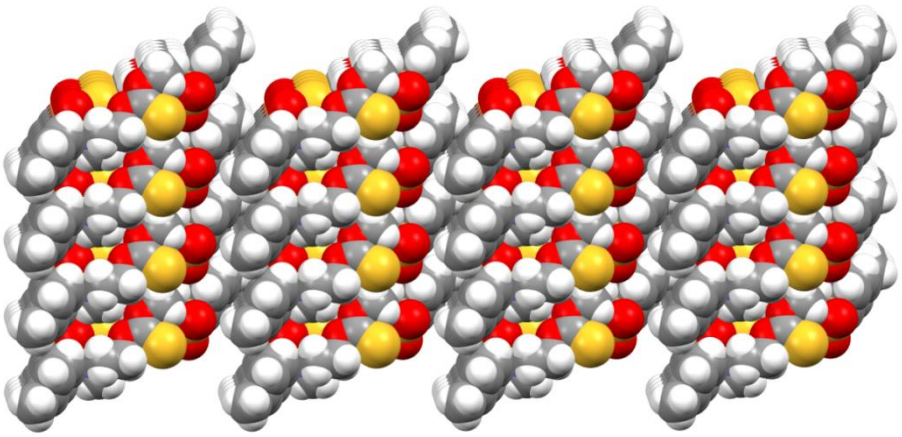

(e)

Figure 9. (a) An ORTEP view of **9** at 40% probability, (b) noncovalent interaction present in **9**, (c) supramolecular aggregate formed through intermolecular weak interactions, (d) Formation of 2D molecular sheet consisting of molecular cavities in **9** through CH...π interactions, (e) All the interactions mutually leading to an 3D infinite assembly of close packed molecules.

3.3.6. Computational Investigations

A DFT level calculation has been performed on diamine precursors $\mathbf{L^1}$-$\mathbf{L^2}$ and binuclear M^{II}xanthate macrocyclic complexes **1-8**. Such calculations have been widely used in recent years due to its ability to provide reasonably good results for huge molecular structures, including transition metal complexes.[22] All the calculations were performed using the Gaussian 03 program suite[23] and molecular orbitals were generated by GaussView 3.0 program. Full geometry optimizations of diamine precursors $\mathbf{L^1}$-$\mathbf{L^2}$ and complexes **1-8** were performed using density functional theory (DFT) at B3LYP/6-31G (d, p) and B3LYP/LanL2DZ basis sets, respectively. Such type of basis set has been used with good success in a number of studies involving similar species, having a good agreement with experimental results.[22] An optimized geometry for the minimum energy conformation of $\mathbf{L^1}$-$\mathbf{L^2}$ and binuclear complexes **1-8** are given in Figure 10 whereas structural parameters are summarized in Table 5.

Table 5. Summary of DFT study performed on **L^1**, **L^2** at the DFT B3LYP/ 6-31G (d, p) level, binuclear M^{II}xanthate complexes **1-8** at the DFT B3LYP/LanL2DZ level and macrocyclic bis-(thiocarbonate O,O-ester) **9** at the DFT B3LYP/ 6-31G (d, p) level.

Comp	Energy of Optimized Geometry (Hartree)	Tranannular M…M Distance (Å)	E_{HOMO}, E_{LUMO} (eV)	$\Delta E_{HOMO-LUMO}$ (eV)	λ_{max} nm calc. (expt.)
L^1	-1183.183	…	-6.5438, -0.9168	5.5846	222 (264)
1	-5992.146	6.886	-6.4801, -1.9538	4.5263	274 (284)
2	-6040.599	5.531	-6.1658, -2.6006	3.5652	348 (354)
3	-6094.255	6.226	-5.9661, -2.1369	3.8292	324 (319)
4	-5833.169	6.832	-6.6880, -1.9434	4.7446	261 (264)
L^2	-708.637	…	-6.3220, -0.5535	5.7685	215 (276)
5	-5043.063	6.736	-6.4777, -1.9540	4.5236	274 (264)
6	-5091.519	5.830	-6.2572, -2.6406	3.6167	343 (319)
7	-5145.174	6.285	-6.0224, -2.0292	3.9933	310 (285)
8	-4884.089	6.866	-6.6562, -1.9206	4.7356	262 (265)

For binuclear M^{II}xanthate macrocyclic complexes **1-8**, optimized geometries clearly suggest that each xanthate ligands bridge two metal centres *via* chelating xanthate moieties, resulting in the formation of binuclear macrocyclic architectures. The optimized structures (Figure 10) clearly suggest the tetrahedral coordination geometry around both the Co^{II} and Zn^{II} nucleus in respective binuclear M^{II}xanthate complexes whereas square planar/distorted square planar coordination geometry around both the Ni^{II} and Cu^{II} centres in their corresponding M^{II}xanthate complexes. The study also points out nearly coplanar macrocyclic ring as minimum energy conformation for all the binuclear M^{II}xanthate complexes and each of the *N*-substituent is projected towards either side of the molecular plane i.e. two *N*-substituents oriented in opposite direction. This unique shape is attained by the molecule to compensate stereo-electronic repulsion associated with the molecular architecture.

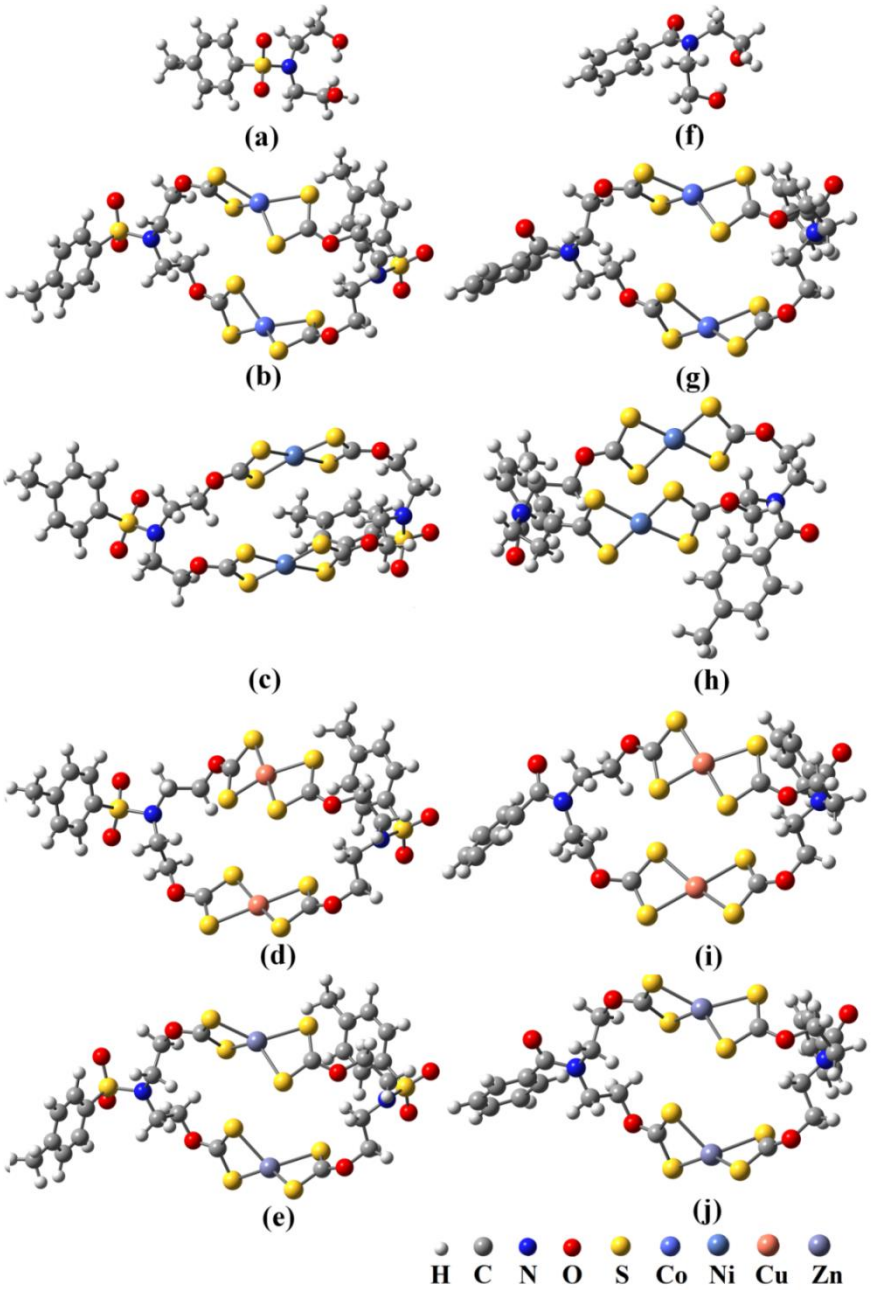

Figure 10. An optimized geometry for the minimum energy conformation of (a) $\mathbf{L^1}$, (b) **1**, (c) **2**, (d) **3**, (e) **4**, (f) $\mathbf{L^2}$, (g) **5**, (h) **6**, (i) **7** and (j) **8**.

The selected structural parameters for the optimized geometries of $\mathbf{L^1}$-$\mathbf{L^1}$ and **1-8** are summarized in Table 6. It appears from the optimized geometries that there is a gradual increase in the bond lengths associated with M^{II}xanthate moieties from Ni-Cu-Zn in all the complexes **2-4**, **6-8** and this trend is indeed unaffected by changing *N*-substituents; however a significant effect of these substituents and metal centre can be seen on C—N—C bond angles. For instance, different C-N-C bond angle is appeared for both the linker units in complexes **1-8** whereas C-N-C bond angles are

appeared to be larger for complexes bearing *N*-Ts substituents (**1-4**) than their *N*-Ts analogues (**5-8**).

Table 6. Selected geometrical parameters obtained from the optimized geometry of $\mathbf{L^1}$-$\mathbf{L^1}$ and **1-8**.

Selected Bond	Bond lengths (Å)	Selected Bonds	Bond angles (º)
		L^1	
O—C	1.415, 1.427	C—N—C	118.93
		L^2	
O—C	1.413, 1.432	C—N—C	118.72
		1	
O—C	1.453-1.457	S—Co—S (chelate)	76.18
C—S	1.716-1.725	S—Co—S (trans S)	122.19-134.73
Co—S	2.396-2.427	C—N—C	118.68, 119.67
		2	
O—C	1.452-1.457	S—Ni—S (chelate)	78.39-78.60
C—S	1.704-1.717	S—Ni—S (trans S)	173.59-177.60
Ni—S	2.276-2.307	C—N—C	119.19, 119.21
		3	
O—C	1.452-1.457	S—Cu—S (chelate)	75.32-75.62
C—S	1.710-1.719	S—Cu—S (trans S)	16290-178.89
Cu—S	2.397-2.422	C—N—C	116.95, 118.93
		4	
O—C	1.451-1.456	S—Zn—S (chelate)	75.77-76.00
C—S	1.720-1.727	S—Zn—S (trans S)	123.09-133.75
Zn—S	2.430-2.475	C—N—C	118.35, 119.49
		5	
O—C	1.450-1.456	S—Co—S (chelate)	76.50-76.68
C—S	1.720-1.725	S—Co—S (trans S)	117.95-125.57
Co—S	2.401-2.430	C—N—C	116.63, 117.58
		6	
O—C	1.449-1.457	S—Ni—S (chelate)	78.46-78.64
C—S	1.706-1.716	S—Ni—S (trans S)	172.73-177.35
Ni—S	2.284-2.304	C—N—C	118.26, 118.68
		7	
O—C	1.449-1.455	S—Cu—S (chelate)	75.49-75.61
C—S	1.710-1.717	S—Cu—S (trans S)	160.52-177.83
Cu—S	2.396-2.423	C—N—C	117.63, 117.83
		8	
O—C	1.449-1.454	S—Zn—S (chelate)	75.83-75.99
C—S	1.716-1.729	S—Zn—S (trans S)	119.03-127.48
Zn—S	2.427-2.487	C—N—C	116.58, 117.53

Table 7. Selected geometrical parameters obtained from X-ray structures.[2]

Selected Bond	Bond lengths (Å)	Selected Bonds	Bond angles (º)
	Binuclear Ni^{II}xanthate complex		
O—C	1.466-1.469	S—Ni—S (chelate)	79.27-79.45
C—S	1.693-1.703	S—Ni—S (trans S)	177.06-178.51
Ni—S	2.210-2.229	coordination geometry	square planar

Further, structural parameters (Table 6) obtained from optimized geometries were compared with those obtained from X-ray study (Table 7) of closely related compounds.[2] It appears that in case of Ni^{II}xanthate complexes **2** and **6**, C-S, M-S bond distances and S—M—S (trans) angles are somewhat overestimated, whereas O-C

bond distances and S—M—S (chelate) bond angles are slightly underestimated compared to the experimental results reported. This slight disparity in the structural parameters could be explained by the mutual effect of differential stereoelectronic factors and the existence of extensive non-covalent interactions.[2] Furthermore, geometry optimization performed on **2** with single crystal geometry as a starting, suggest that the molecular conformation obtained in solid state is not a minimum energy conformation in gas phase (0.488 Hartree) which is indeed stabilized by large number of noncovalent interactions as depicted by X-ray study.

The molecular electrostatic potential (MESP) of any chemical species provides valuable information about electronic environment of the molecule, useful for the prediction of its properties and potential sites for reactivity, including biological systems.[14] The localization of slight negative potential around >SO_2/>CO moieties whereas absence of localization of any charge in vicinity to the metal centres could be clearly revealed from mapping of electrostatic potential surface. This generates a scope for development of macrocycle with varied cavity size and electronic environment for effective interaction, for instance hydrogen bonding with various guest molecules including biomolecules.

Moreover, an investigation of frontier molecular orbitals becomes essential for speculation of the potential reactivity of the molecule due to their vital contribution in the photo-physical properties, especially localization and the HOMO–LUMO energy gap.[25] The calculated HOMO-LUMO energy gaps (Isovalue = 0.02) for ligand precursor $\mathbf{L^1}$, $\mathbf{L^2}$ and binuclear M^{II}xanthate complexes **1**-**8** are given in Table 2 and their localization is illustrated in Figure 11.

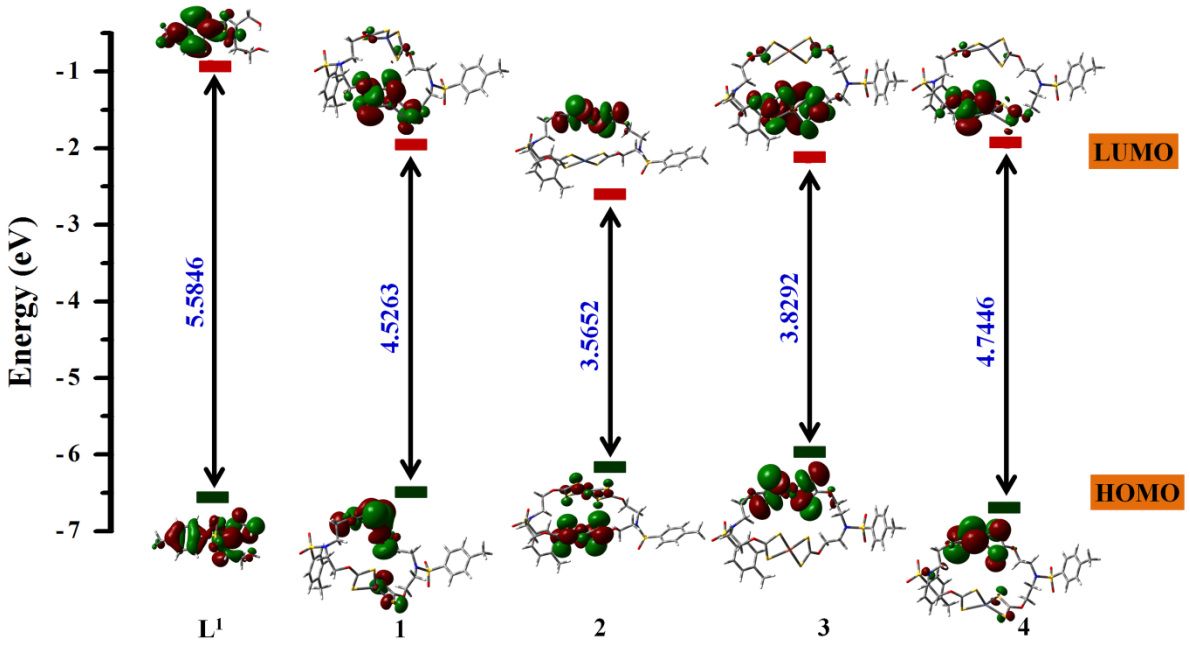

(a)

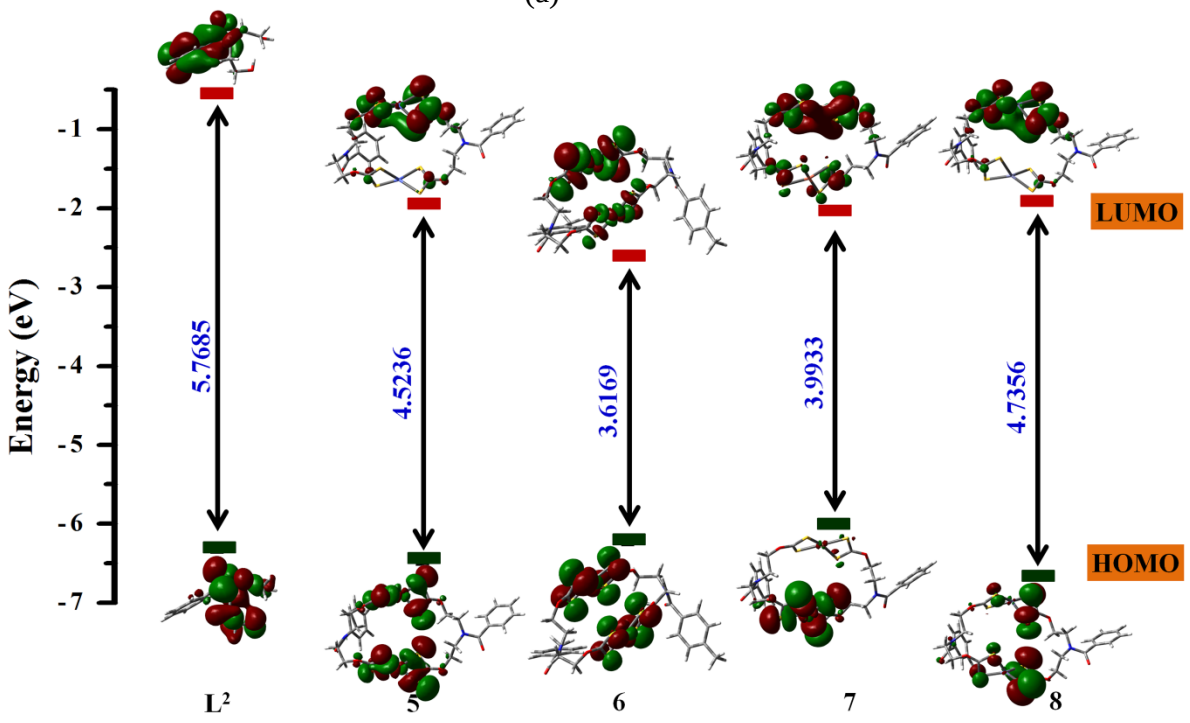

(b)

Figure 11. Frontier molecular orbitals (Isovalue= 0.02) for (a) **L**[1] and **1-4**, (b) **L**[2] and **5-8.**

It may be noted that for **L**[1]**-L**[2], the HOMO is localized over alkyl chain and LUMO is delocalized over aromatic ring. However, in case of the M^{II}xanthate complexes HOMO as well as LUMO (Figure 11b) is predominantly localized over coordinated xanthate functionality. The HOMO-LUMO energy differences for the Ni^{II}xanthates **2** (3.5652 eV) and **6** (3.6169 eV) are significantly lower compared to their $Co^{II}/Cu^{II}/Zn^{II}$ analogues. These complexes follow HOMO-LUMO energy gap

trend as **4**>**8**>**1**>**5**>**3**>**7**>**6**>**2**. The structural parameters and localization of frontier orbitals are almost similar in both solid as well as gas phase, for instance, one coordinated xanthate moiety contribute for HOMO while other one contribute for HOMO to small extent and predominantly for LUMO with comparable HOMO-LUMO band gaps. Additionally, the calculated HOMO-LUMO energy difference for binuclear complexes **1-8** are significantly lower, compared to their corresponding ligand precursors which falls in the range 3.5-4.5 eV, suggestive of the semiconducting nature of these compounds[26] and thus increases the potential applicability of this class of compounds towards semiconducting materials. Generally, the computational investigations are validated by the analogous experimental results; in this work the calculated HOMO-LUMO gaps for complexes **1-8** are clearly supported by their corresponding UV-visible absorption data showing comparable λ_{max} values .

Bis-(thiocarbonate O,O-ester) macrocyclic (9):

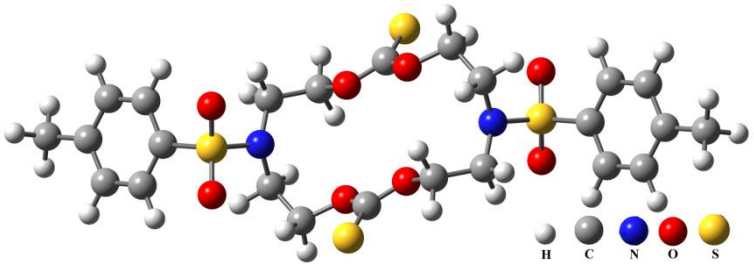

Figure 12. An optimized geometry of **9**.

Geometry optimization by DFT study performed on **9** with single crystal geometry as a starting, suggest that the molecular conformation obtained in solid state is not a minimum energy conformation in gas phase (0.478 Hartree).(Figure 12) The large number of noncovalent interaction such as CH...π, CH...O, CH...S, etc are essentially stabilizing the relatively higher energy conformation in solid state. The structural parameters and localization of frontier orbitals are almost similar in both solid as well as gas phase, as HOMO is delocalized over –OCSO- moiety and LUMO is delocalized over both the peripheral phenyl rings. However, HOMO-LUMO band gap is slightly lower for conformation attained in solid state. (Figure 13)

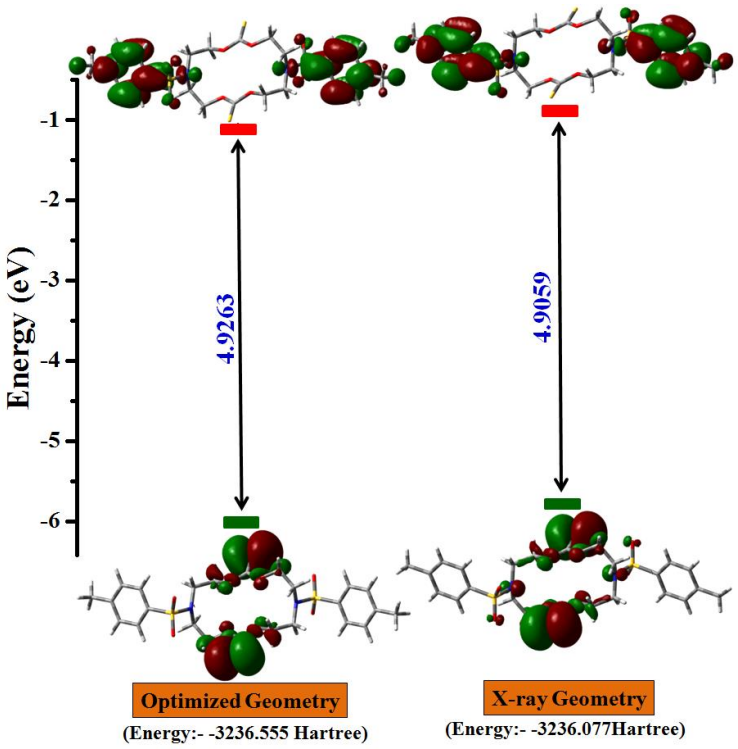

Figure 13. Frontier molecular orbitals (Isovalue= 0.02) for **9** at minimum energy conformation and X-ray geometry.

3.3.7. *In vitro* Cytotoxicity

An excellent cytotoxic activity of complexex bearing 1,1'-dithio ligands has inspired us to design similar compounds in search of better potency. Literature evidences a wide range of macrocyclic natural product and their synthetic derivatives have long been clinically used because of the high degree of potency as well as selectivity achieved by these scaffolds.[27] Despite of metal based macrocyclic complexes widely studied in supramolecular chemistry, especially host-guest reactivity study,[28] this structural class is surprisingly underexploited in medicinal chemistry. Hence, it was pertinent to investigate binuclear M^{II}xanthate macrocyclic scaffolds **1-8** for their potential anticancer activity by the MTT assay[5] against the malignant human cancer cell lines HEP 3B (Hepatoma) and IMR 32 (Neuroblastoma) and compare their cyctotoxicity with clinically used antineoplastic drug cisplatin. The IC_{50} values shown in Table 5 represent 50 % inhibition concentration against the malignant tumor cell lines were obtained after treatment of M^{II}xanthate macrocycles for 14 h with HEP 3B and IMR 32 cells. (Table 8, Figure 14)

Table 8: *In vitro* cytotoxicity IC_{50} (μM) by MTT assay for entry **1-17** against HEP 3B and IMR 32 cancer cell lines.

Entry	Compound	HEP 3B IC_{50} Value (μM/mL)	IMR 32 IC_{50} Value (μM/mL)
1	L (DEA)	154.08±5.33	186.04±18.07
2	L^1	120.47±0.77	71.84±6.01
3	L^2	88.41±5.73	69.78±6.31
4	1	59.98±3.51	44.31±2.75
5	2	11.21±0.33	19.86±1.6
6	3	88.35±13.53	83.91±10.88
7	4	14.21±0.63	17.09±1.37
8	5	47.32±4.74	23.31±3.11
9	6	62.89±8.25	49.69±10.64
10	7	90.89±13.12	70.46±11.12
11	8	4.98±0.8	7.54±1.0
12	9	10.34±1.39	15.78±1.87
13	$Co(OAc)_2.4H_2O$	262.04±0.84	343.18±17.14
14	$Ni(OAc)_2.4H_2O$	373.93±2.29	342.79±15.99
15	$Cu(OAc)_2.H_2O$	29.85±2.90	19.03±2.85
16	$Zn(OAc)_2.2H_2O$	212.12±2.69	192.26±7.61
17	Cisplatin	56.56±3.93	61.99±5.2

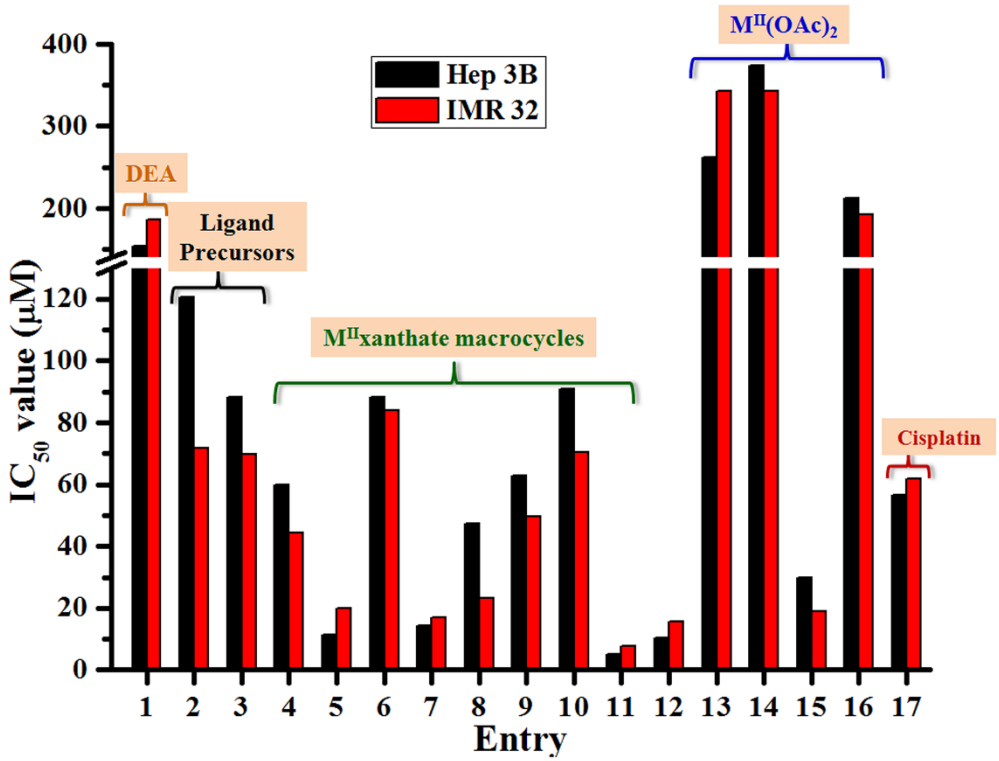

Figure 14. *In vitro* cytotoxicity *i.e.* IC_{50} for compound **1-17** against **HEP 3B and IMR 32** cancer cell lines.

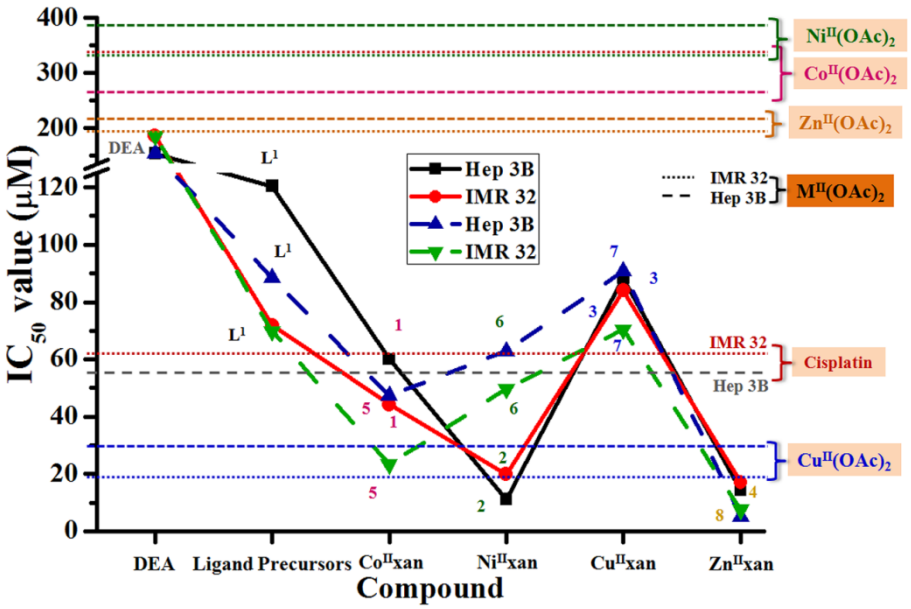

Figure 15. Effect of the change in **'*R*'** group and ***'metal centre'*** towards cytotoxicity against **HEP 3B** and **IMR 32** cancer cell lines.

The enhancement in cytotoxicity is observed upon incorporation of *N*-substituent in diethanol amine (**L**), in which *N*-Bz substituent display more cytotoxic character. The trend of cytotoxicity is reversed upon incorporation of *N*-substituent in **L**, for instance **L** is more cytotoxic to HEP 3B cells than IMR 32 cells whereas $\mathbf{L^1}$-$\mathbf{L^2}$ both are more cytotoxic towards IMR 32 cells. The binuclear M^{II}xanthate complexes follows cytotoxicity trends as **8**>**2**>**4**>**5**>**1**>**6**>**3**>**7** against HEP 3B and **8**>**4**>**2**>**5**>**1**>**6**>**7**>**3** against IMR 32 cell lines. The differential reactivity profile and hence potency of **1-8** against HEP 3B and IMR 32 cell lines is mainly associated with unique molecular conformation adopted by the macrocyclic scaffolds. (Figure 15) The extremely lower potency of metal salts is associated with their ionic nature which become the barrier for the membrane transportation and hence, for the resultant cytotoxic activity. Interestingly, all the binuclear M^{II}xanthate macrocycles found extremely active against both the cell lines HEP 3B and IMR 32 than their corresponding metal acetates, except $Cu^{II}(OAc)_2$. The higher potency of all the complexes **1-8** is probably due to the predominant reactivity of chelated xanthate moiety in biological systems. Among all the binuclear M^{II}xanthate macrocycles **1-8**, complexes bearing Zn^{II} and Ni^{II} centres display better cytotoxic activity, and project the binuclear Zn^{II}xanthate macrocycles **8** with optimum potency. Furthermore, comparison of the IC_{50} values of screened binuclear macrocycles with the clinically used antineoplastic drug cisplatin clearly underlines the greater potency of some

complexes (**2**, **4**, **5** and **8**) against both the cancer cell lines, more than 5-10 folds in some cases. The macrocyclic bis-(thiocarbonate O,O-ester) **9** also display higher cytotoxic activity with lower IC_{50} values 10.34±1.39 (HEP 3B) and 15.78±1.87 (IMR 32) than ligand precursors and cisplatin against both the cell lines. In recent days, theoretical calculation is a one of the robust tool used to study structure-activity relationship (SAR)[29] which offers structural and stereo-electronic parameters, useful to get mechanistic insights into the transport of the compound across the cell membranes and possible interactions with biological macromolecules. The surface potential of the molecule is also crucial suggesting the potential sites for non-covalent interactions for instance, hydrogen bonding with biological receptors resulting into the effective cellular membrane transportation. It appears that binuclear Zn^{II}xanthate macrocycle **4** and **8** with highest charge on sulfur atoms (-0.126 to -0.161 e.u. for **4** and (-0.127 to -0.172 e.u. for **8**) and higher HOMO-LUMO energy difference (4.7446 eV for **4** and 4.7356 eV for **8**) exhibits optimum cytotoxicity among all the binuclear M^{II}xanthate macrocycles and suggests its higher reactivity in the biological conditions leading to the enhanced potency. The better cytotoxicity of binuclear xanthate macrocyclic complexes could be due to their accessibility for transchelation reactions with biomolecules and transmetallation reaction with metal ions present at the site of action which alters the hard/soft properties, the lipophilic/hydrophilic balance of the resulting complexes as well as hydrogen bonding with biomolecules which ultimately help to permeate the cellular membrane.

Our hypothesis on binuclear M^{II}xanthate complexes that might involve multiple mode of action leading to the cell death can be explained by several previously observed effects of isostructural dithiocarbamate complexes. 1,1-dithio moieties are known to exert cytotoxicity through antiangio-genesis effects, inhibition of numerous metalloenzymes and NF-KB-related gene-expression and modulation of cellular metabolism, which lead to tissue damage.[30] The decomposition and metabolic products of a transition metal 1,1-dithio complexes in vivo, *ca* free 1,1-dithio moieties, CS_2 are reportedly able to arrest the cell proliferation.[31] Dou and co-workers reported several studies concerning the cytotoxic activity of discrete, transition metal complexes.[32] Electrochemical and stability data[33] suggests that the most stable dithiocarbamate complexes proved to be most cytotoxic *in vitro* and also against the cisplatin-resistant. Recent investigations highlights the electronic density analysis of

different dithiocarbamate metal complexes to correlate their toxicity as well as the ability to inhibit proteasome and induce apoptosis in human cancer cells.[34] It has appeared that the dithiocarbamate complexes holding higher electronic density over sulfur atom within the complex are more active against the JAMM domain of the 26S proteasome.[34] Due to presence of almost similar structural and electronic features in dithiocarbamate and xanthate complexes, analogous mode of action for the antitumor activity could be expected for both of them. Beyond this, the possibility of transchelation reactions with physiological molecules and metabolic products of xanthate complexes could alter the intracellular metal constitutions which lead to the cytotoxic activity. Further, anticancer potential of cobalt, nickel, copper and zinc complexes reportedly attained by the interaction with DNA and some DNA-binding proteins.[35]

3.4. Conclusions

The study allows us to conclude that a series of binuclear metallamacrocyclic complexes [M^{II}_2-μ^2-bis-{(κ^2S,S-$S_2COCH_2CH_2)_2N(R)$}] {R = Ts and M = Co^{II} **1**, Ni^{II} **2**, Cu^{II} **3**, Zn^{II} **4**; R = Bz and M = Co^{II} **5**, Ni^{II} **6**, Cu^{II} **7**, Zn^{II} **8**} can be efficiently synthesized in a one-pot self-assembling process involving *N*-substituted diethanol amine precursors $\mathbf{L^1}$ or $\mathbf{L^2}$, CS_2 and metal acetate. All the complexes exhibit fluorescent property and maximum fluorescence intensity is recorded for binuclear Zn^{II}xanthate macrocycles**.** Complex **4** has been utilized to synthesize a macrocyclic compound, 6,14-ditosyl-1,3,9,11-tetraoxa-6,14-diaza-cyclohexadecane-2,10-dithione (**9**), which is extremely difficult to synthesize conventionally. The single crystal X-ray study reveals the unambiguous structures **2** and **9** and it further explain the packing patterns of molecules in the solid state. The coordination sphere at Ni^{II} centre is square planar and flexible alkyl chain lead to a strain free macrocyclic architecture. This study allows us to propose a novel synthetic methodology for the synthesis of organic macrocyclic compounds which are extremely difficult to synthesize conventionally. The DMSO/DMF solution of **2** exhibit reversible charge transfer induced thermochromism in temperature range 30-90 ºC (DMSO) and 30-60 ºC (DMF). This is the first report on exploitation of binuclear 1,1'-dithio complexes in thermochromism. Computational investigations performed on the model compounds reinforced the experimental outcomes and provides valuable information about

frontier molecular orbitals. The enhanced cytotoxic activities of some of the the macrocyclic scaffolds **1-8** against human cancer HEP 3B and IMR 32 cells, as compared to cisplatin, a well known antineoplastic drug makes these compounds biologically significant. Thus, the current study projects an efficient approach to enhance the antiproliferative activity via self assembly process and provides a guideline for the development of a class of compounds having high potency against the human cancer cell lines.

3.5. References

1. Beer, P. D.; Berry, N. G.; Cowley, A. R.; Hayes, E. J.; Oates, E. C.; Wong, W. W. H. *Chem. Commun*., **2003**, 2408. (b) Fox, O. D.; Cookson, J.; Wilkinson, E. J. S.; Drew, M. G. B.; MacLean, E. J.; Teat, S. J.; Beer, P. D. *J. Am. Chem. Soc*. **2006**, *128*, 6990. (c) Cookson, J.; Beer, P. D. *Dalton Trans.*, **2007**, 1459.
2. Beer, P. D.; Cowley, A. R.; Jeffery, J. C.; Paul, R. L.; Wong, W. W. H. *Polyhedron* **2003**, *22*, 795.
3. (a) William, C.; Ray, I.; Grinstaff, M. W. *Macromolecules* **2003**, *36*, 3557. (b) Albertson, A.-C.; Sjoling, M. *J. Macromol. Sci., Part A* **1992**, *29*, 43. (3) Feng, J.; He, F.; Zhuo, R. X. *Macromolecules* **2002**, *35*, 7175.
4. Wang, H.-F.; Su, W.; Zhang, C.; Luo, X.-h.; Feng, J. *Biomacromolecules* **2010**, *11*, 2550.
5. Manosroi, J.; Dhumtanom, P.; Manosroi, A. *Cancer Lett.* **2006**, *235*, 114.
6. (a) Liao, L.-Y.; Shen, G.; Zhang, X.; Duan, X.-F. *Green Chem*., **2012**, *14*, 695. (b) Zhao, W.; Carreira, E. M. *Org. Lett*. **2011**, *13*, 5084.
7. Lesage, S. *J. Agric. Food Chem.* **1980**, *28*, 787.
8. Ercolani, G. *J. Phys. Chem. B* **2003**, *107*, 5052.
9. (a) Jones, C. J. *Chem. Soc. Rev.* **1998**, *27*, 289. (b) Leininger, S.; Olenyuk, B.; Stang, P. *Chem. Rev.* **2000**, *100*, 853.
10. G. W. Watt and B. J. McCormick, *Spectrochim. Acta*, **1965**, *21*, 753.
11. Bonati, F.; Ugo, R. *J. Organomet. Chem*., **1967**, *10*, 257.
12. Andotra, S.; Kalgotra, N.; Pandey, S. K. *Bioinorg. Chem. Appl*. **2014**, *2014*, 12, Article ID 780631.
13. Verma, S. K.; Singh, V. K. *Polyhedron* **2014**, *76*, 1.

14. Sreedaran, S.; Bharathi, K. S.; Rahiman, A. K.; Jagadish, L.; Kaviyarasan, V.; Narayanan, V. *Polyhedron* **2008**, *27*, 2931.
15. (a) Lee, K.-H.; Choi, C.-S.; Jeon, K.-S. *J. Photosci.* **2002**, *9*, 71. (b) Martens, S. C.; Zschieschang, U.; Wadepohl, H.; Klauk, H.; Gade, L. H. *Chem. Eur. J.* **2012**, *18*, 3498. (c) Valdés, A. C.; P.-Luis, G.; Rivero, I. A. *J. Mex. Chem. Soc*. **2007**, *51*, 87. (d) Madrigal, D.; C.; P.-Luis, G.; Rivero, I. A. *J. Mex. Chem. Soc*. **2006**, *50*, 175. (e) Liu, H.; Li, B.; Liu, D.; Xu, Z. *Chem. Phys. Lett*. **2001**, *350*, 441. (f) Mizobe, Y.; Hinoue, T.; Yamamoto, A.; Hisaki, I.; Miyata, M.; Hasegawa, Y.; Tohnai, N. *Chem. Eur. J*. **2009**, *15*, 8175. (g) Reddy, D. R.; Maiya, B. G. *J. Porphyrins Phthalocyanines* **2002**, *06*, 3.
16. Queen, M. S. Towey, B. D. Murray, K. A. Veldkamp, B. S. Byker, H. J. Szilagyi, R. K. Coord. Chem. Rev. 2013, 257, 564.
17. Memon, A. A.; Afzaal, M.; Malik, M. A.; Nguyen, C. Q.; O'Brien, P.; Raftery, J. *Dalton Trans.* **2006**, 4499.
18. Kumar, S. S.; Selvi, T. R. *Synth. React. Inorg. Met.-Org. Nano-Met. Chem.* **2008**, *38*, 710.
19. Onwudiwe, D. C.; Ajibade, P. A. *Int. J. Mol. Sci*. **2011**, *12*,1964.
20. ''CrysAlispro'' program (Version 1.171.37.33 Agilent Technologies, 2014).
21. Sheldrick, G.M. SHELXL-97: program for crystal structure refinement, University of Göttingen, Göttingen, Germany, 1997.
22. Salehzadeh, S.; Bayat,M. *Comp. Theor.Chem*. **2011**, *965*, 131.
23. Frisch, M. J.; Trucks, G. W.; Schlegel, H. B.; Scuseria, G. E.; Robb, M. A.; Cheeseman, J. R.; Montgomery Jr., J. A.; Vreven, T.; Kudin, K. N.; Burant, J. C.; Millam, J. M.; Iyengar, S. S.; Tomasi, J.; Barone, V.; Mennucci, B.; Cossi, M.; Scalmani, G.; Rega, N.; Petersson, G. A.; Nakatsuji, H.; Hada, M.; Ehara, M.; Toyota, K.; Fukuda, R.; Hasegawa, J.; Ishida, M.; Nakajima, T.; Honda, Y.; Kitao, O.; Nakai, H.; Klene, M.; Li, X.; Knox, J. E.; Hratchian, H. P.; Cross, J. B.; Adamo, C.; Jaramillo, J.; Gomperts, R.; Stratmann, R. E.; Yazyev, O.; Austin, A. J.; Cammi, R.; Pomelli, C.; Ochterski, J. W.; Ayala, P. Y.; Morokuma, K.; Voth, G. A.; Salvador, P.; Dannenberg, J. J.; Zakrzewski, V. G.; Dapprich, S.; Daniels, A. D.; Strain, M. C.; Farkas, O.; Malick, D. K.; Rabuck, A. D.; Raghavachari, K.; Foresman, J. B.; Ortiz, J. V.; Cui, Q.; Baboul, A. G.; Clifford, S.; Cioslowski, J.; Stefanov, B. B.; Liu, G.; Liashenko, A.; Piskorz, P.; Komaromi, I.; Martin, R. L.;

Fox, D. J.; Keith, T.; A.-Laham, M. A.; Peng, C. Y.; Nanayakkara, A.; Challacombe, M.; Gill, P. M. W.; Johnson, B.; Chen, W.; Wong, M. W.; Gonzalez, C.; Pople, J. A.; Gaussian, Inc., Wallingford, CT, **2004**.

24. (a) Gadre, S. R.; Bhadane, P. K. *Resonance*, **1999**, *4*, 11. (b) Bulat, F. A.; T.-Labbé, A.; Brinck, T.; Murray, J. S.; Politzer, P. *J Mol Model* **2010**, *16*, 1679. (c) Politzer, P.; Laurence, P. R.; Jayasuriya, K. *Environ. Health Perspect.* **1985**, *61*, 191.
25. Vladimirova, K. G.; Freidzon, A. Y.; Kotova, O. V.; Vaschenko, A. A.; Lepnev, L. S.; Bagatur'yants, A. A.; Vitukhnovskiy, A. G.; Stepanov, N. F.; Alfimov, M. V. *Inorg. Chem.* **2009**, *48*, 11123.
26. Kadu, R.; Singh, V. K.; Verma, S. K.; Raghavaiah, P.; Shaikh M. M. *J Mol. Struct*. **2013**, *1033*, 298.
27. (a) Driggers, E.M.; Hale, S. P.; Lee, J.; Terrett, N. K. *Nat. Rev. Drug Discov.* **2008**, *7*, 608. (b) Mallinson, J.; Collins, I. *Future Med. Chem.* **2012**, *4*, 1409. (c) Mann A. Conformational restriction and/or steric hindrance in medicinal chemistry. In: *The Practice Of Medicinal Chemistry*, Wermuth CG (Ed.). Academic Press, London, UK 2008.
28. (a) Beer, P. D. *Acc. Chem. Res.* **1998**, *31*, 71. (b) E.-Aroussi, B.; Guénée, L.; Pal, P.; Hamacek, J. *Inorg. Chem.* **2011**, *50*, 8588.
29. (a) Piazzi, L.; Cavalli, A.; Belluti, F.; Bisi, A.; Gobbi, S.; Rizzo, S.; Bartolini, M.; Andrisano, V.; Recanatini, M.; Rampa, A. *J. Med. Chem*. **2007**, *50*, 4250. (b) Ferreira, I. P.; de Lima, G. M.; Paniago, E. B.; Rocha, W. R.; Takahashi, J. A.; Pinheiro, C. B.; Ardisson, J. D. *Eur. J. Med. Chem*. **2012**, *58*, 493. (c) Soares, M. A.; Lessa, J. A.; Mendes, I. C.; Da Silva, J. G.; dos Santos, R. G.; Salum, L. B.; Daghestani, H.; Andricopulo, A. D.; Day, B. W.; Vogt, A.; Pesquero, J. L.; Rocha, W. R.; Beraldo, H. *Bioorg. Med. Chem*. **2012**, *20*, 3396. (d) Parrilha, G. L.; da Silva, J. G.; Gouveia, L. F.; Gasparoto, A. K.; Dias, R. P.; Rocha, W. R.; Santos, D. A.; Speziali, N. L.; Beraldo, H. *Eur. J. Med. Chem*. **2011**, *46*, 1473.
30. (a) Bach, S. P.; Chinery, R.; O'Dwyer, S. T.; Potten, C. S.; Coffey, R. J.; Watson, A. J. *Gastroenterology* **2000**, *118*, 81. (b) Daniel, K. G.; Chen, D.; Orlu, S.; Cui, Q. C.; Miller, F. R.; Dou, Q. P. *Breast Cancer Res.* **2005**, *7*, R897. (c) Segovia, N.; Crovetto, G.; Lardelli, P.; Espigares, M. J. Appl. Toxicol. 2002, 22, 353. (d) Viquez, O. M.; Valentine, H. L.; Amarnath, K.; Milatovic, D.; Valentine, W. M.

Toxicol. Appl. Pharmacol. 2008, 229, 77. (e) Chabicovsky, M.; P.-Grassauer, E.; Seipelt, J.; Muster, T.; Szolar, O. H. J.; Hebar, A.; Doblhoff-Dier, O. Basic Clin. Pharmacol. Toxicol. 2010, 107, 758. (f) Nagy, E. M.; Sitran, S.; Montopoli, M.; Favaro, M.; Marchiò, L.; Caparrotta, L.; Fregona, D. *J Inorg. Biochem*. **2012**, *117*, 131. (g) Qian, Y.; Ma, G.-Y.; Yang, Y.; Cheng, K.; Zheng, Q.-Z.; Mao, W.-J.; Shi, L.; Zhao, J.; Zhu, H.-L. *Bioorg. Med. Chem*. **2010**, *18*, 4310.

31. (a) Amarnath, V.; Amarnath, K.; Valentine, W. M. *Curr. Top. Toxicol.* **2007**, *4*, 39. (b) Garcia, J. I.; Humeres, E. *J. Org. Chem.* **2002**, *67*, 2755. (c) Humeres, E.; Debacher, N. A.; Franco, J. D.; Lee, B. S.; Martendal, A. *J. Org. Chem.* **2002**, *67*, 3662. (d) Humeres, E., Debacher, N. A., and Sierra, M. M. *J. Org. Chem.* **1999**, *64*, 1807.
32. (a) Milacic, V.; Chen, D.; Ronconi, L.; Landis-Piwowar, K. R.; Fregona, D.; Dou, Q. P. *Cancer Res.* **2006**, *66*, 10478–10486. (b) Chen, D.; Cui, Q. Z. C.; Yang, H. J.; Dou, Q. P. *Cancer Res.* **2006**, *66*, 10425–10433. (c) Daniel, K. G.; Gupta, P.; Harbach, R. H.; Guida, W. C.; Dou, Q. P. *Biochem. Pharmacol.* **2004**, *67*, 1139. (d) Chen, D.; Frezza, M.; Shakya, R.; Cui, Q. C.; Milacic, V.; Verani, C. N.; Dou, Q. P. *Cancer Res.* **2007**, *67*, 9258. (e) Daniel, K. G.; Chen, D.; Orlu, S.; Cui, Q. C.; Miller, F. R.; Dou, Q. P. *Breast Cancer Res*. **2005**, *7*, R897. (f) Chen, D.; Peng, F.; Cui, Q. C.; Daniel, K. G.; Orlu, S.; Liu, J.; Dou, Q. P. *Front. Biosci*. **2005**, *10*, 2932.
33. Keter, F. K.; Guzei, I. A.; Nell, M.; van Zyl, W. E.; Darkwa, J. *Inorg. Chem*. **2014**, *53*, 2058.
34. (a) Cvek, B.; Milacic, V.; Taraba, J.; Dou, Q. P. *J. Med. Chem*. **2008**, *51*, 6256. (b) Milacic, V.; Chen, D.; Giovagnini, L.; Diez, A.; Fregona, D.; Dou, Q. P. *Toxicol. Appl. Pharmacol*. **2008**, *231*, 24.
35. (a) M. N.; Patel, M. R.; Chhasatia, Gandhi, D. S. Bioorg. *Med. Chem. Lett*. **2009**, *19*, 2870. (b) Wang, X.-Y.; Zhang, J.; Li, K.; Jiang, N.; Chen, S.-Y.; Lin, H.-H.; Huang, Y.; Ma, L.-J.; Yua, X.-Q. *Bioorg. Med. Chem*. **2006**, *14*, 6745. (c) Buchtik, R.; Travnicek, Z.; Vanco, J.; Herchel, R.; Dvorak, Z. *Dalton Trans*. **2011**, *40*, 9404. (d) Bhat, S. S.; Kumbhar, A. A.; Heptullah, H.; Khan, A. A.; Gobre, V. V.; Gejji, S. P.; Puranik, V. G. *Inorg. Chem*. **2011**, *50*, 545. (e) G.-Gimenez, L. J.; G.-Alvarez, M.; L.-Gonzalez, M.; Macias, B.; Borras, J.; Alzuet, G. *J. Inorg. Biochem*. **2009**, *103*, 923. (f) Buchtik, R.; Travnicek, Z.; Vanco, J. *J.*

Inorg. Biochem. **2012**, *116C*, 163. (g) Arjmand, F.; Muddassir, M. *Chirality* **2011**, *23*, 250. (h) Chin, L. F.; Kong, S. M.; Seng, H. L.; Khoo, K. S.; Vikneswaran, R.; Teoh, S. G.; Ahmad, M.; Khoo, S. B. A.; Maah, M. J.; Ng, C. H. *J. Inorg. Biochem*. **2011**, *105*, 339. (i) Takeshima, T.; Ikeda, M.; Yokoyama, M.; Fukada, N.; Muraoka, M. *J. Chem. Soc., Perkin* **1979**, *1*, 692. (j) Beaty, J. A.; Jones, M. M.; Wilson, D. J.; Ma, L. *Chem. Res. Toxicol.* **1992**, *5*, 568.

3.6. Annexure

3.6.1. Spectral Characterization:

NMR Spectra:

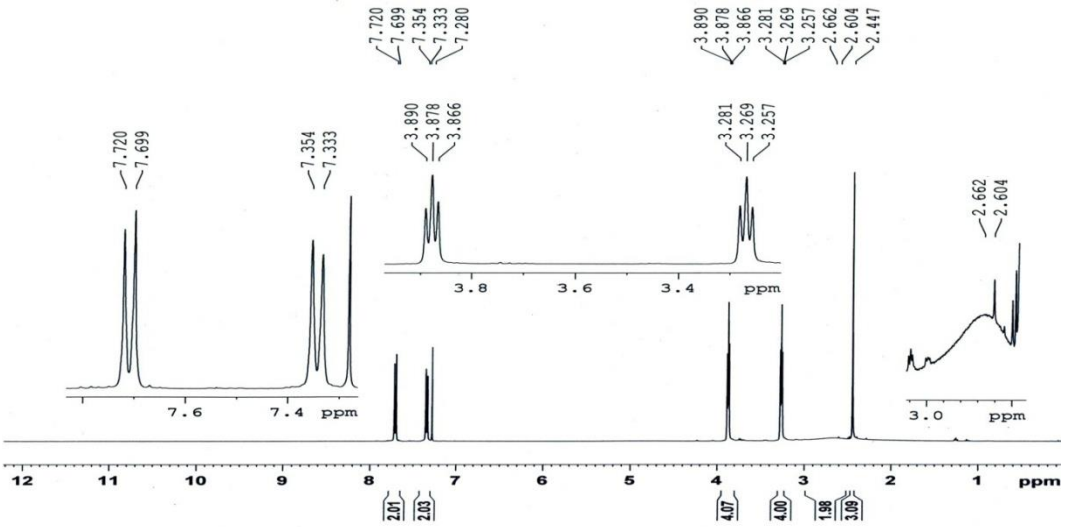

Annexure 1.[1]H NMR of **L[1]**.

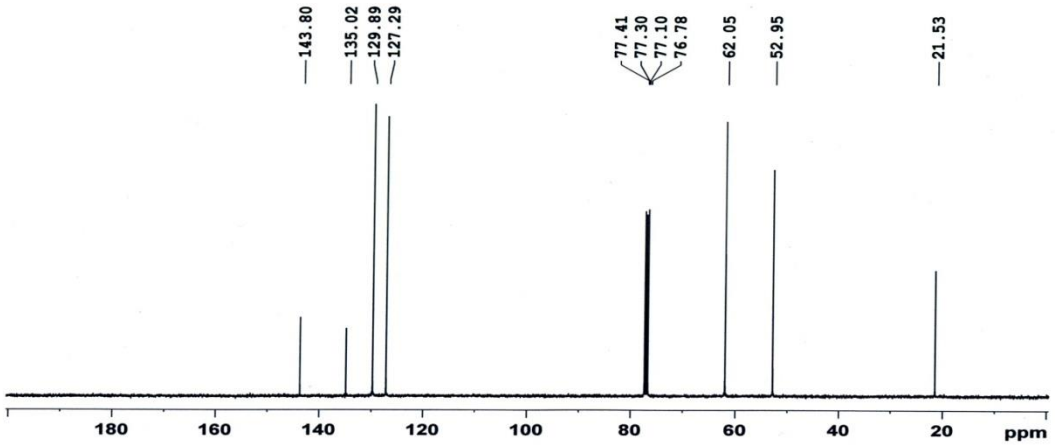

Annexure 2.13C NMR of **L1**.

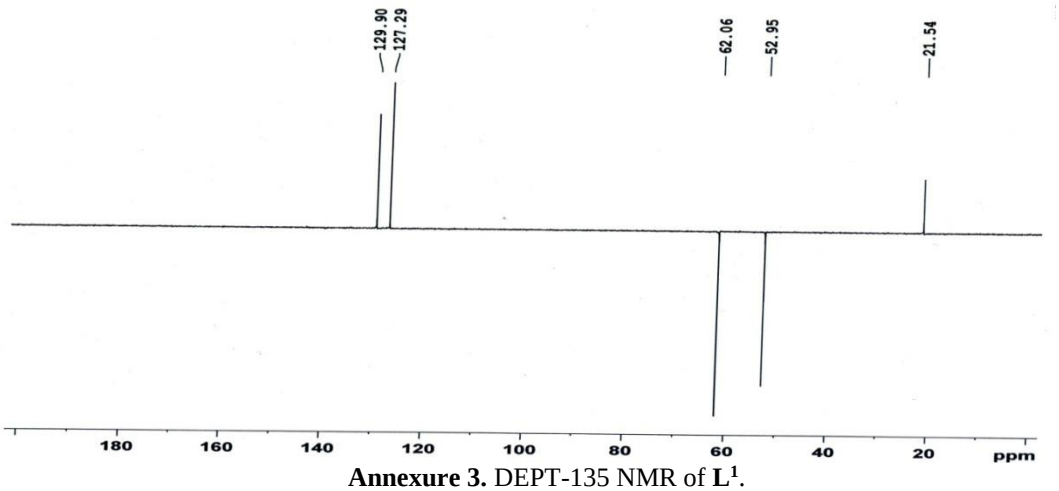

Annexure 3. DEPT-135 NMR of **L[1]**.

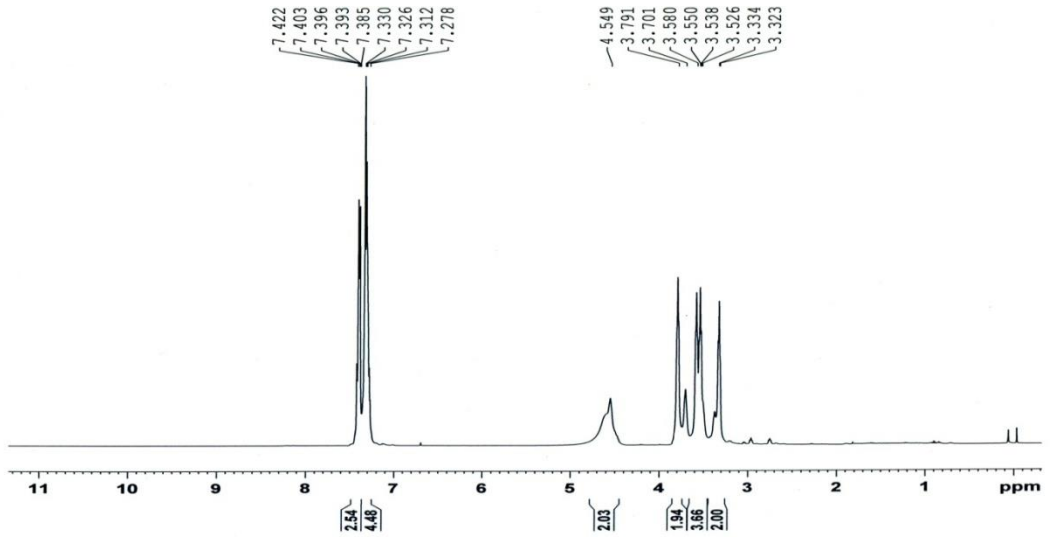

Annexure 4.[1]H NMR of **L[2]**.

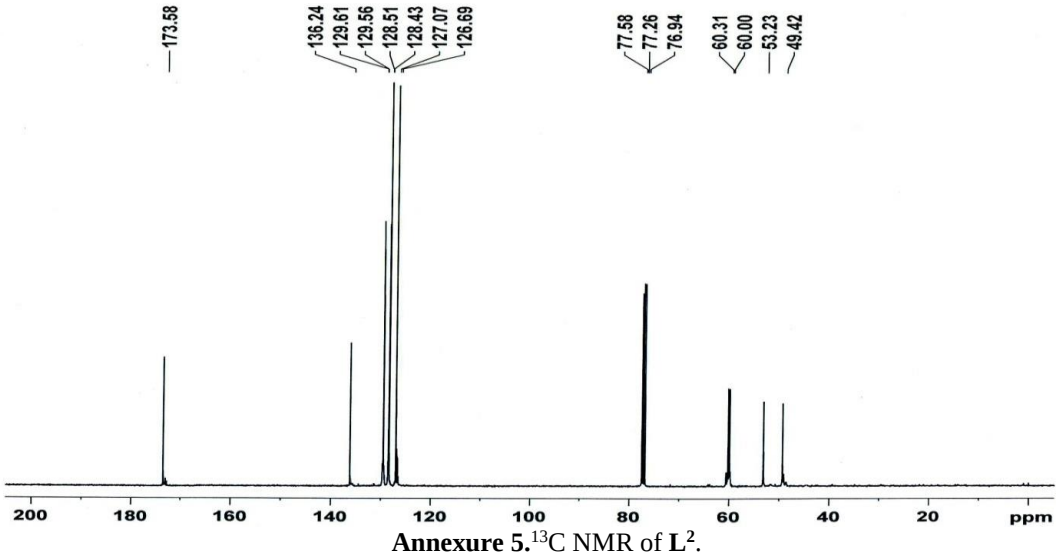

Annexure 5.[13]C NMR of **L[2]**.

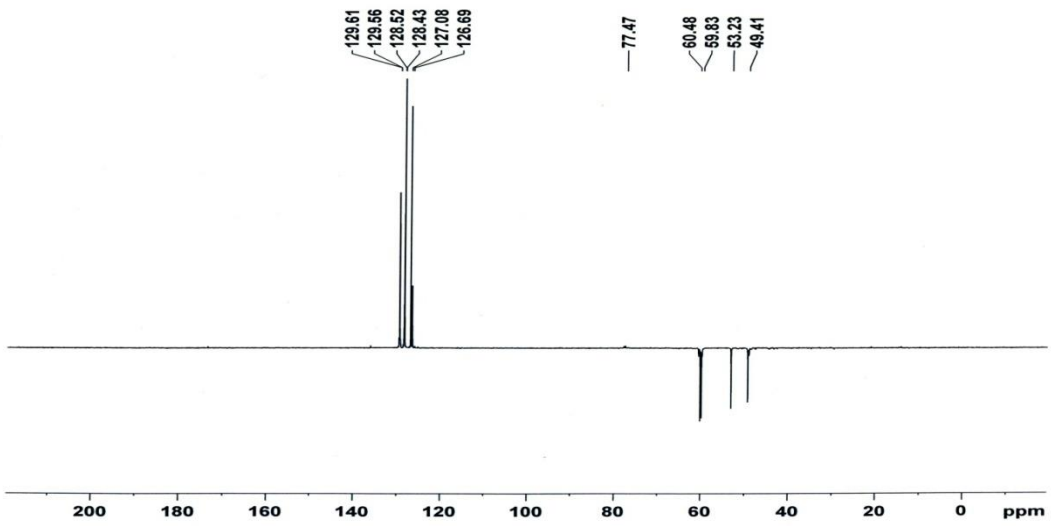

Annexure 6. DEPT-135 NMR of **L**[2].

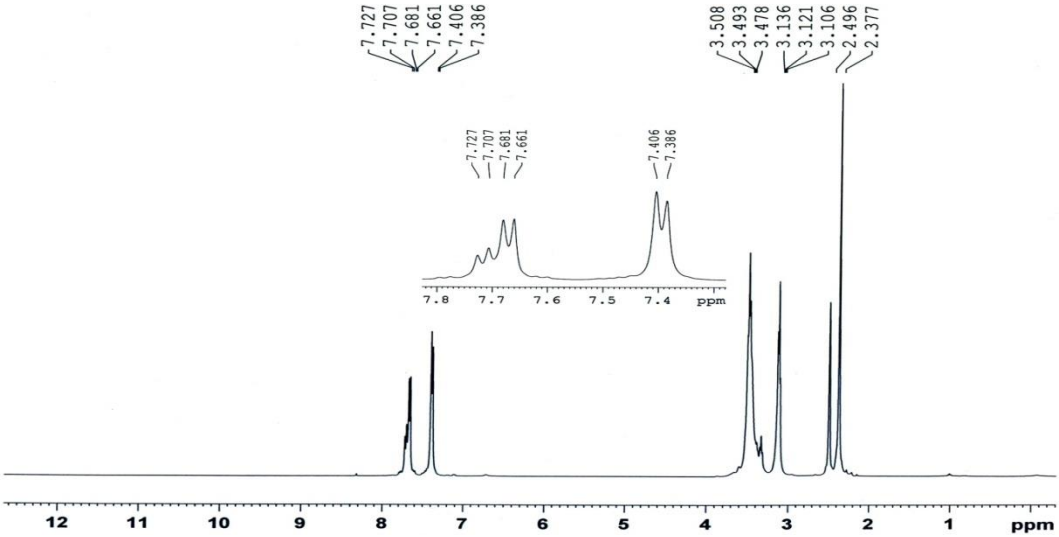

Annexure 7.[1]H NMR of **4**.

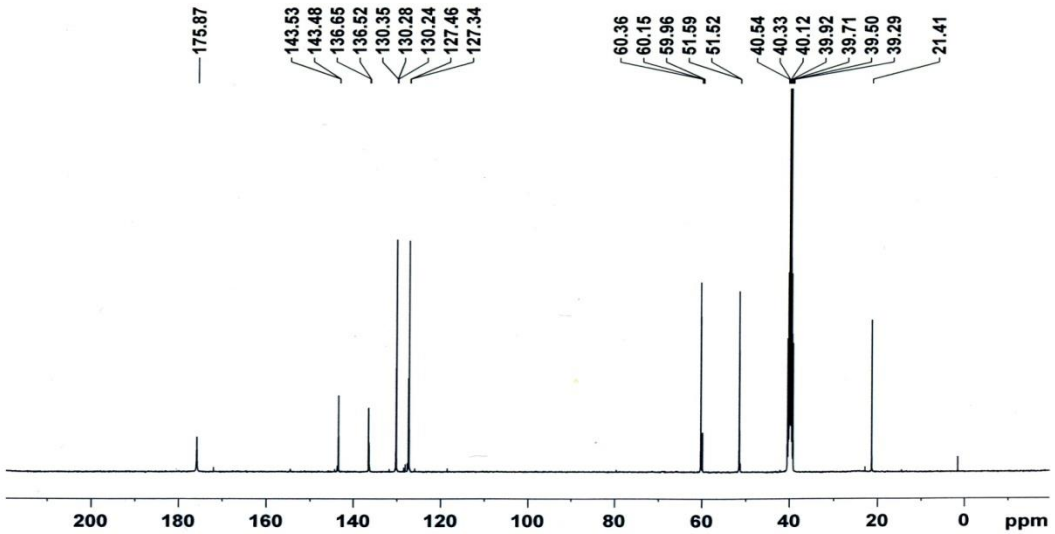

Annexure 8.[13]C NMR of **4**.

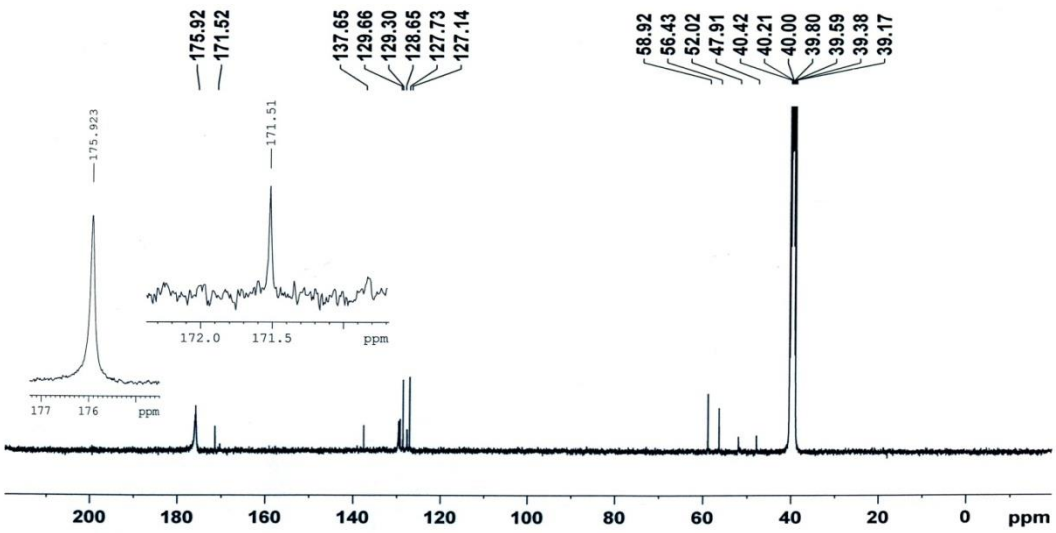

Annexure 9.[13]C NMR of **8**.

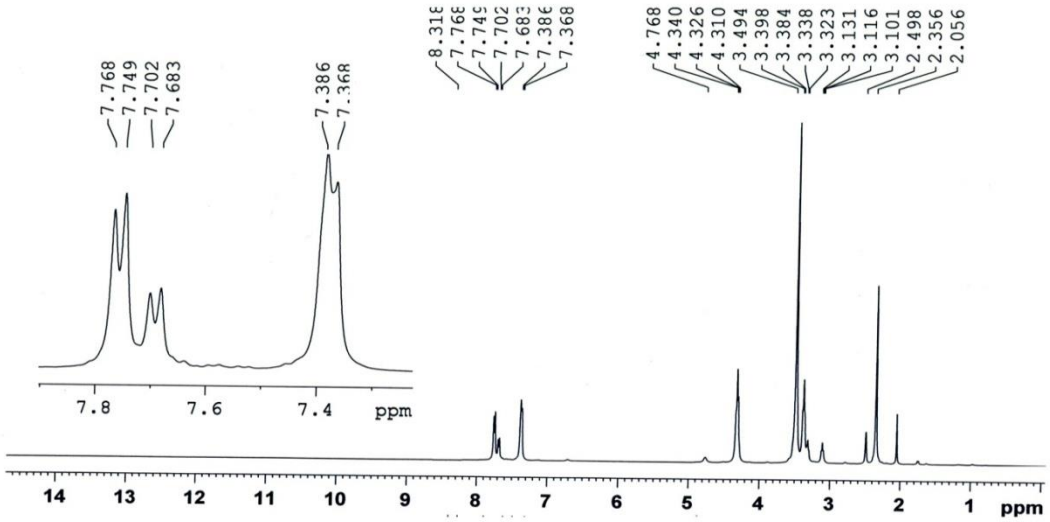

Annexure 10.[1]H NMR of **KxanL[1]**.

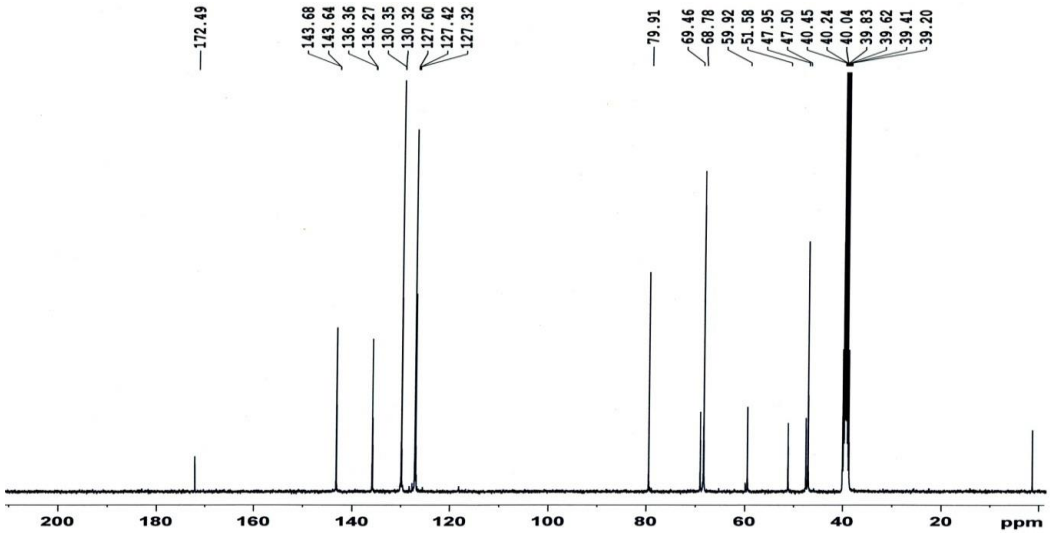

Annexure 11.[13]C NMR of **KxanL[1]**.

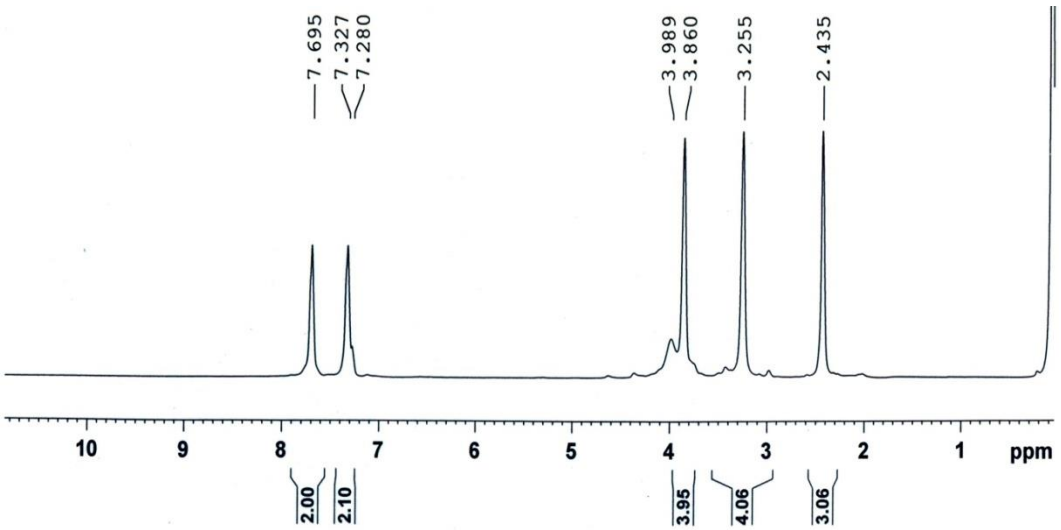

Annexure 12.[1]H NMR of **9**.

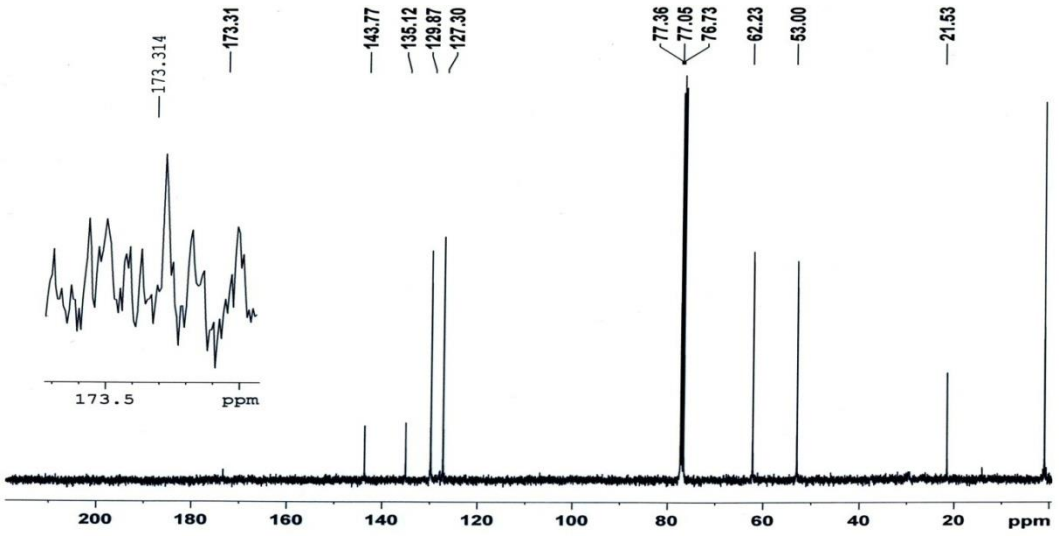

Annexure 13.[13]C NMR of **9**.

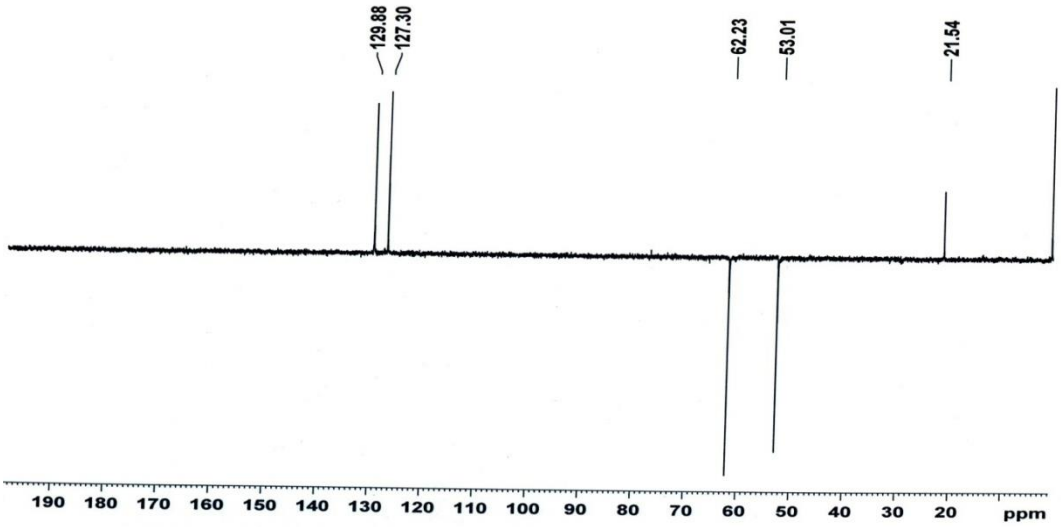

Annexure 14.DEPT-135 NMR of **9**.

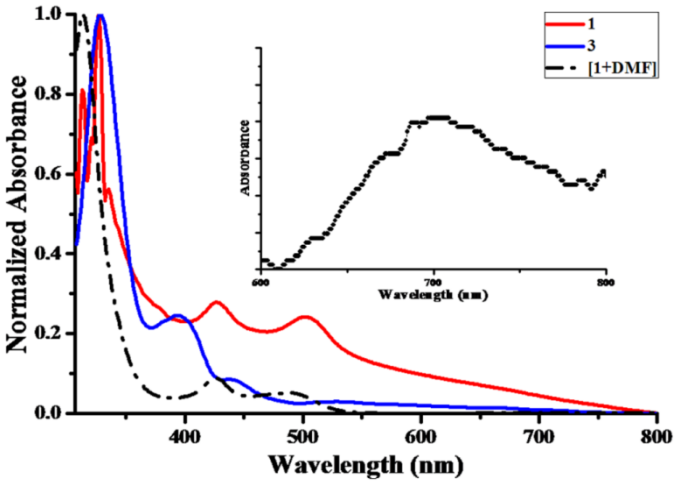

Annexure 15..UV-Visible spectra of **2** and **6** in CH_2Cl_2 solution.

3.6.2. Thermogravimetric Analysis:

Table A1: Thermogravimetric analysis of **L^1-L^2**, and **1-4**.

Entry	DTA (°C) (µV)	DTG (°C) (µg/min)	Significant Mass loss % (temp range °C)	Inference
L^1	96.8 (-11.01)	287.4 (960)	96.8% (200-400) 98.1 % (50-550)	DTA peak at 96.8 °C due to melting. 1st stage: single stage mass loss due to evaporation. Maximum rate of mass loss observed at 287.4 °C on DTG curve.
L^2	74.2 (2.06), 239 (19.9), 276.6 (19.55), 348.8 (16.95)	74.7 (48), 145.9 (55), 296 (975), 392.3 (57)	95.4% (150-400) 99.1 % (50-550)	1st stage: insignificant mass loss of solvent impurities up to 100 °C. 2nd stage: single stage mass loss due to evaporation. Maximum rate of mass loss observed at 296 °C on DTG curve.
1	181.1 (24.23) 214.4 (27.91)	182.2 (74.7) 211.7 (337.9) 250.4 (246.8)	72.5 % (150-400) 74.3 % (50-550)	1st-2nd stage: multi stage mass loss due to removal of organic fragments. Stable residual mass of 25.7 % correspond to NiS (calc. 19.4 %) and small amount of char. Maximum rate of decomposition observed at 211.7 °C on DTG curve.
2	62.0 (-13.6) 285.2 (38.19) 379.2 (35.86) 428.3 (36.48) 488 (17.62)	64.1 (256.6) 278.2 (446.0) 361.0 (99.5) 464.8 (184.6)	28.5 % (50-300) 42.5 % (50-550)	1st-2nd stage: multi stage mass loss due to removal of organic fragments. 3rd stage: decomposition continues after 550 °C. Maximum rate of decomposition observed at 278.2 °C on DTG curve.
3	75.3 (-8.9) 166.9 (35.09) 231.7 (31.42) 371.3 (36.36) 387.9 (35.82) 467.5 (19.44)	75.9 (217.6) 358.1 (195.8) 378.3 (112.5) 460.6 (116.4)	13.9 % (50-150) 28.1 % (150-400) 6.8 % (400-550) 49.5 % (50-550)	1st-2nd stage: multi stage mass loss due to removal of organic fragments. 3rd stage: decomposition continues after 550 °C. Maximum rate of decomposition observed at 75.9 °C on DTG curve.
4	269.6 (40.43) 325.5 (27.55) 412.5 (23.43)	56.0 (163) 271.5 (168.9) 441.7 (60)	45.6 % (50-300) 54.5 % (50-550)	1st stage: continuous multi stage mass loss due to removal of organic fragments and decomposition continues after 550 °C. Maximum rate of decomposition observed at 271.5 °C on DTG curve.

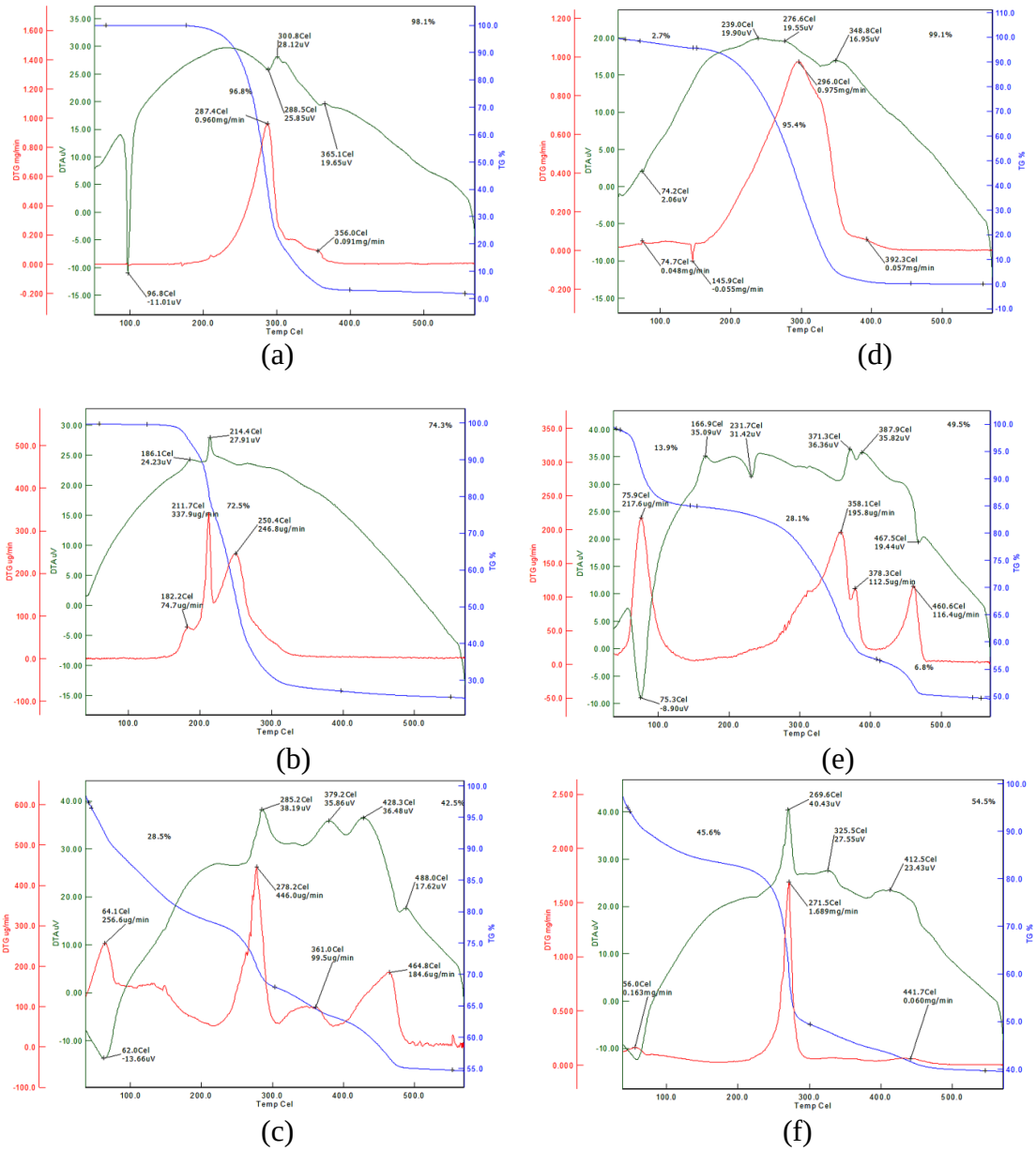

Annexure 16..TG-DTA plots for **1-8**.

3.6.3. Computational Investigations:

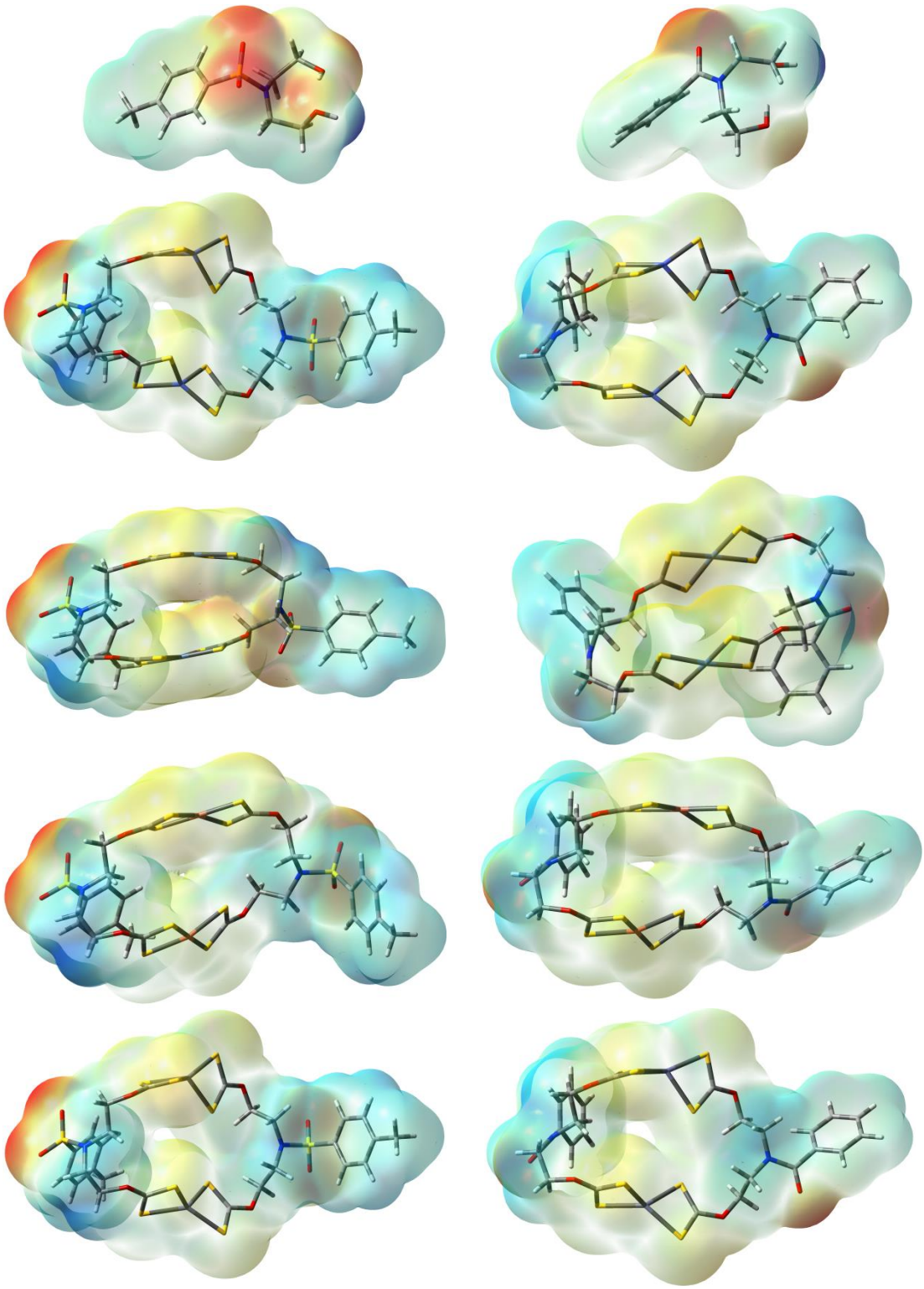

Annexure 17..MESP diagram for **1-8**.

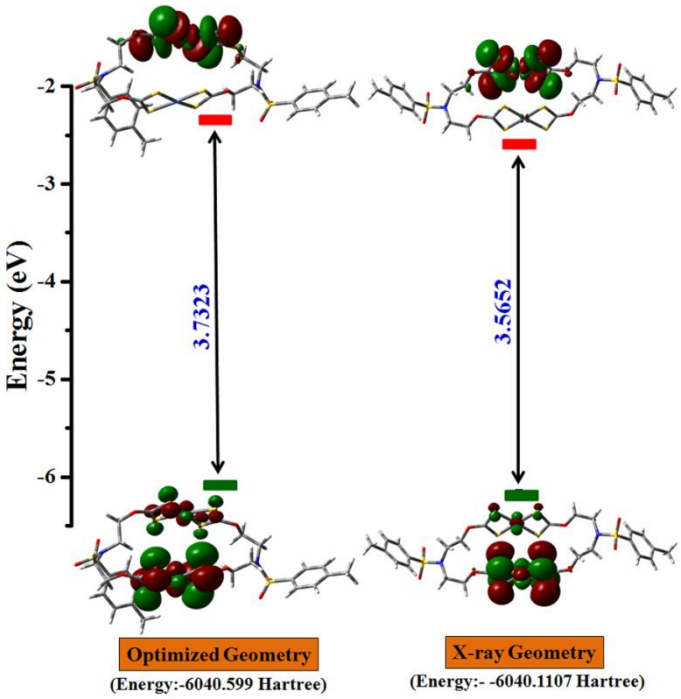

Annexure 18..Frontier orbitals for **2**.

3.6.4. *In vitro* cytotoxicity:

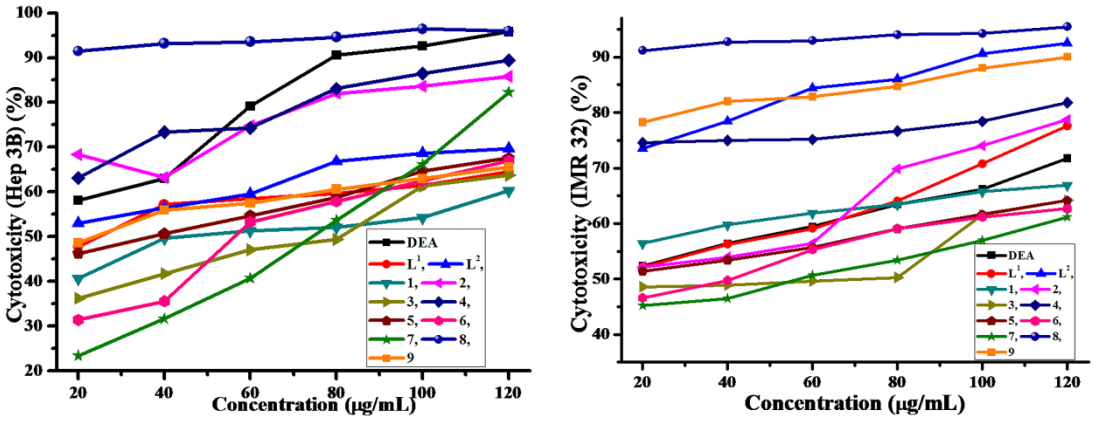

(a) (b)

Annexure 16..% inhibition of cell growth against HEP 3B and IMR 32 for L^1-L^2 and **1-9**.

Table A2. Parameters obtained from the computational investigations and cytotoxic activity for electronic models.

Entry	E_{HOMO}, E_{LUMO} (eV)	$\Delta E_{HOMO-LUMO}$ (eV)	Charges on 'N' and chelated 'N-CSS-M' atoms	M...M distance (Å)	Dipole moment (Debye)
DEA			O: - (0.548-0.560)	...	2.4537
L^1	-6.5438, -0.9168	5.5846	O: - (0.524-0.569)	...	6.4730
L^2	-6.3220, -0.5535	5.7685	O: - (0.528-0.565)	...	2.5624
1	-6.4801, -1.9538	4.5263	Co: (0.060-0.061) S: - (0.022-0.076) C: (0.080-0.088) O: - (0.377-0.386)	6.886	5.5671
2	-6.1658, -2.6006	3.5652	Ni: - (0.245-0.258) S: (0.012-0.073) C: (0.072-0.092) O: - (0.380-0.396)	5.531	7.0141
3	-5.9661, -2.1369	3.8292	Cu: - (0.090-0.098) S: (-0.032- +0.025) C: (0.074-0.086) O: - (0.380-0.385)	6.226	7.6653
4	-6.6880, -1.9434	4.7446	Zn: (0.519-0.527) S: - (0.126-0.161) C: (0.055-0.066) O: - (0.378-0.385)	6.832	5.5540
5	-6.4777, -1.9540	4.5236	Co: (0.080-0.081) S: - (0.018-0.071) C: (0.078-0.085) O: - (0.375-0.384)	6.736	4.6199
6	-6.2572, -2.6406	3.6167	Ni: - (0.253-0.256) S: (0.004-0.070) C: (0.077-0.091) O: - (0.380-0.396)	5.830	2.4282
7	-6.0224, -2.0292	3.9933	Cu: - (0.086-0.103) S: (-0.030- +0.026) C: (0.074-0.081) O: - (0.377-0.385)	6.285	3.4562
8	-6.6562, -1.9206	4.7356	Zn: (0.510-0.529) S: - (0.127-0.172) C: (0.051-0.061) O: - (0.375-0.384)	6.866	4.7291
9	-6.0295, -1.1031	4.9263	S: - (0.237) C: (0.416) O: - (0.408-0.423)	...	0.0000